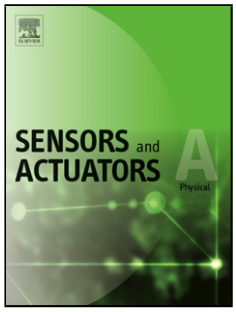


# Design and characterisation of a compact 4-degree-of-freedom fast steering mirror system based on double Porro prisms for laser beam stabilization

Yu-Hao Chang (Writing - original draft) (Conceptualization) (Methodology) (Software) (Validation), Guangbo Hao (Conceptualization) (Writing - review and editing), Chien-Sheng Liu (Writing - review and editing) (Supervision) (Project administration)

PII: S0924-4247(21)00101-1

DOI: https://doi.org/10.1016/j.sna.2021.112639

Reference: SNA 112639

To appear in: *Sensors and Actuators: A. Physical*

Received Date: 8 September 2020

Revised Date: 3 January 2021

Accepted Date: 18 February 2021

Please cite this article as: { doi: https://doi.org/

Journal Pre-proof

# Design and characterisation of a compact 4-degree-of-freedom fast steering mirror system based on double Porro prisms for laser beam stabilization

**Yu-Hao Chang**[1]

Department of Mechanical Engineering, National Chung Cheng University

Address: No.168, University Road, Minhsiung Township, Chiayi County 621301, Taiwan

Tel: +886-5-2720411, E-mail: tako79716@gmail.com

**Guangbo Hao** [2]

School of Engineering, University College Cork, Ireland

Address: Electrical Building 1.06, College Road, Cork, Ireland

Tel: +353(0)21 490 3793, E-mail: G.Hao@ucc.ie

**Chien-Sheng Liu** [3, *]

Department of Mechanical Engineering, National Cheng Kung University

Address: No.1, University Road, Tainan City 701, Taiwan

Tel: +886-6-2757575, E-mail: csliu@mail.ncku.edu.tw

***Corresponding author: csliu@mail.ncku.edu.tw**



Graphical abstract

Design a new compact 4-DOF actuator to implement the idea of fast steer mirror (FSM) based on double Porro prisms and integrate the proposed FSM compensation system of our previous study.

Journal Pre-proof

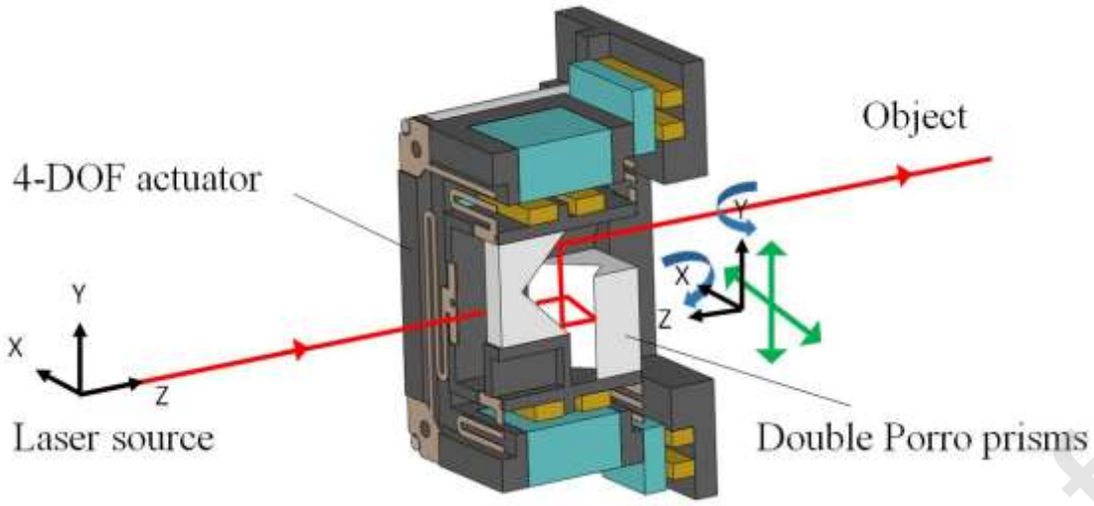


## Highlights

- Propose a 4-degree-of-freedom (DOF) actuator to integrate the proposed fast steer mirror (FSM) compensation system of our previous study
- Design and analyze the characteristics of the electromagnetic structure and mechanical structure for the proposed 4-DOF FSM.
- Verify the laser error compensation of proposed 4-DOF FSM by using a laboratory-built prototype.
- The experiment results show that the proposed 4-DOF FSM has the rotational and translational ranges of ± 5 mrad and ± 0.04 mm along the X and Y axes, respectively, and the bandwidths of 10 Hz and 39 Hz for rotational and translational motions, respectively

## ABSTRACT

This paper proposes a 4-degree-of-freedom (DOF) actuator for a fast steer mirror (FSM) compensation system in order to compensate for 4-DOF laser errors. The mathematic system modeling was built to design and predict the performance of the proposed 4-DOF FSM. Finite element analysis was performed by using a commercial software to analyze the characteristics of the electromagnetic structure and mechanical structure for the proposed 4-DOF FSM. This study further verifies the properties of the proposed 4-DOF FSM by using a laboratory-built

Journal Pre-proof

prototype. The proposed 4-DOF FSM has the travel range of ±5 mrad and ±0.04 mm along X and Y axes with accuracy of 0.025 mrad and 0.0012 mm and the bandwidth of rotational part and translational part are 10 Hz and 39 Hz, respectively.

Keywords: Fast steer mirror, Laser beam stabilization, Voice coil motor, 4 degree-of-freedom actuator, Flexure structure

## 1. Introduction

Lasers can benefit high directionality and coherence, which are widely utilized in our daily life and different technological fields, such as optical disk drives, laser surgery, laser rangefinder, and laser cutting [1-6]. However, a laser beam is a directionality light source that can not change its direction by itself. Therefore, an optical device of fast steer mirror (FSM) was invented to steer laser beam for different purposes in different fields [7-9].

FSM has been applied in free-space optical communications [10], scanning [11], laser cutting, laser tracker [12, 13] and laser beam stabilization [14]. Based on our previous observation, when we used optical measuring instruments to measure the six-degree-of-freedom geometric errors of a linear motion stage, the laser spot of optical measuring instruments would drift due to air flow, temperature change and machine vibration in the working environment. Thus the measurement accuracy of the optical measuring instruments is significantly affected. The above issue can be addressed by designing a laser beam stabilization system using FSM, which is the main motivation of this paper.

The commercial FSM only has two degree-of-freedom (DOF) to steer laser beam tilting along X- and Y-axe, which consists of a mirror, an actuator and a flexure structure [15-20]. The mirror would be rotated along X- or Y- axis when the actuator is actuated. The voice coil motor (VCM) is most common actuator utilized to rotate the mirror in the FSM, because it has the advantages of simple structure, low cost, robust performance, and high productivity characteristics [21-24]. The flexure structure plays a role to balance the loads and suspend the moving parts of the

Journal Pre-proof

FSM. Spring plates are widely used as the flexure structure in the FSM because of easy fabrication and low cost [25-28]. Therefore, the FSM performance is strongly related to its actuator and flexure structure.

In our previous study [29], we proposed a 4-DOF FSM based on double Porro prisms, which could steer laser beam to translate along X- and Y-directions and tilt about X- and Y- directions. The double Porro prisms are variants of the 90° prisms that are used as a pair to displace and invert a beam [30]. The double Porro prisms based FSM has the advantage that could have different cutting grooves using laser cutting depending on the demand of customer, and also has the advantage of shorter optical path length, fewer elements, and easier set-up at different locations in laser beam stabilization [29]. However, in [29] only a 4-DOF FSM concept and optical design were presented without designing a 4-DOF motion stage/actuator. Therefore, the performances of this 4-DOF FSM were verified by using a commercial 6-axis Hexapod motion stage. The resulting FSM system is bulky when integrating the commercial 6-axis Hexapod stage and the double Porro prisms.

Based on the above advance, this study we aim to design a new compact 4-DOF actuator to implement the idea of FSM based on double Porro prisms, and to integrate all parts in a very compact configuration (to the best of our knowledge, there is no 4-DOF FSM on the market). We will design a hybrid flexure structure to balance the actuation loads and suspend the moving parts of the FSM. Note that for the purpose of a compact integration, the desired 4-DOF motion is enabled by the special arrangements of electromagnetic actuators rather than by mobility design of the flexure structure, i.e., the flexure structure is not a 4-DOF flexure mechanism in principle.

## 2. Design of proposed 4-DOF FSM

The common commercial 2-axis FSM is composed of VCMs and spring plates, which has the advantages of high dynamic performance and simple/compact structure characteristics. Therefore, this study continues to use simple structure characteristics to balance the loads and suspend the

Journal Pre-proof

moving parts of the FSM and aims to design a 4-axis FSM. In addition, the similar VCM structure is also applied in the optical image stabilization (OIS) cameras module [31] which used spring plates and elastic strings to achieve focusing and OIS, respectively. This study integrates the multi-axis actuators of the camera module with the double Porro Prisms, and proposes a new 4-DOF FSM that has 4-DOF motions to steer laser beam. Figure 1 shows its operating principle. As shown, in the middle of the proposed 4-DOF FSM, there is a tunnel, inside which double Porro Prisms are set. Therefore, a laser beam could pass through the proposed 4-DOF FSM and reflect to the object by the double Porro Prisms, and the laser beam will be steered to a different direction when the 4-DOF actuation system is controlled.

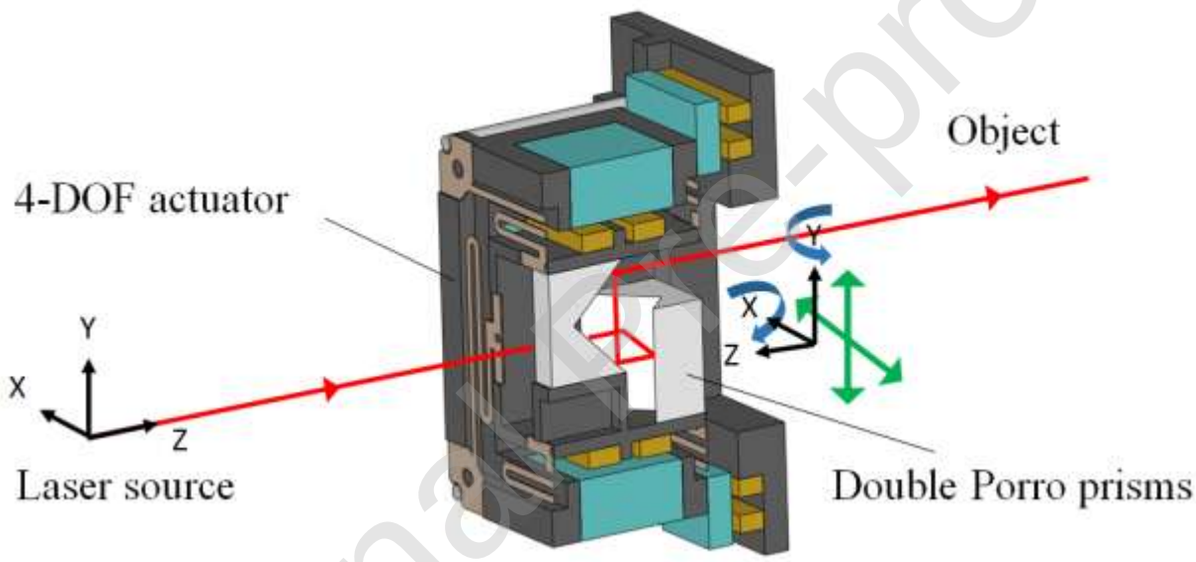


Figure 1. Laser steering principle of proposed 4-DOF FSM.

Figure 2 shows the detailed design of the proposed 4-DOF FSM, which is a serial motion system with two moving masses, the prism holder and the magnet holder. As shown, double Porro prisms and four coils are directly fixed on the prism holder. Eight magnets are fixed on the magnet holder. There are another four coils being fixed on the base. The prism holder is embedded into a magnet holder, and they are compliantly connected via the two-layer in-parallel spring plates. The magnet holder is compliantly connected to the base via the four elastic strings. The spring plates suspend the double Porro Prisms and make the gap between the coils and magnets. The elastic

Journal Pre-proof

strings suspend the magnet holder and create the gap between the coils and magnets. The magnet holder carrying the prism holder can translate in the X- and Y-directions by electrifying the four coils fixed to the base. The prism holder can rotate separately about the X- and Y-directions by electrifying the four coils fixed to the magnet holder.

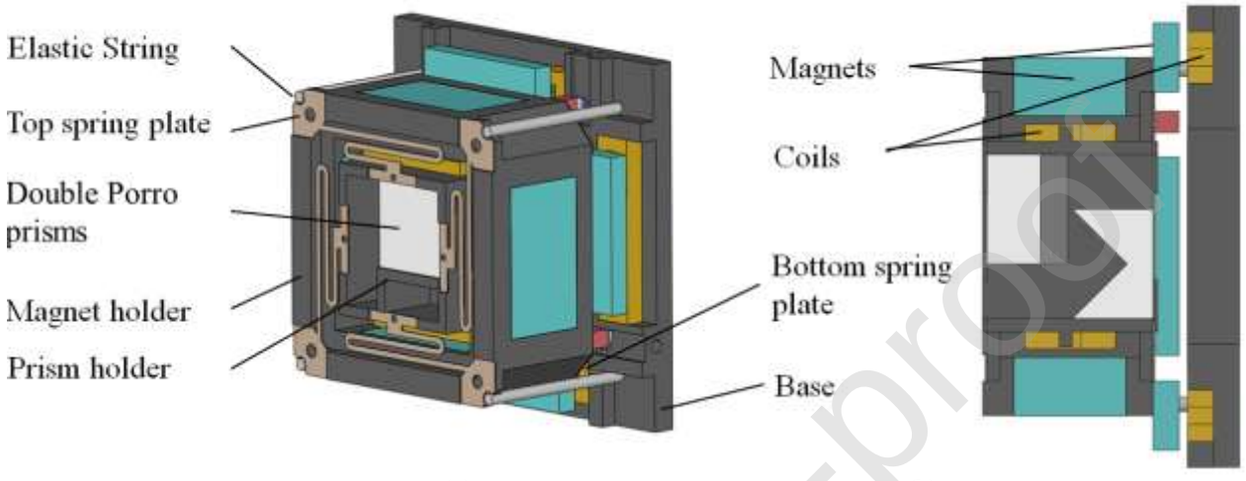


Figure 2. The FSM system: (a) 3D model and (b) sectional view of proposed 4-DOF FSM structure.

Figure 3 depicts the generation of actuation forces of the proposed 4-DOF FSM to steer the double Porro Prisms for rotation and translation 4-DOF. As shown in Fig. 3(a), when a pair of opposite-direction electric currents are passed through the coils on the magnet holder, a pair of opposite-direction Lorentz forces $F_{VCM}$ (and therefore a torque) are generated at the both sides of the prism holder to rotate the prism holder, and furthermore to tilt the laser beam. Figure 3(a) refers to one rotational VCM actuation. Likewise, as shown in Fig. 3(b), when a pair of electric currents are passed through the coils on the base, a pair of same-direction $F_{VCM}$ are generated at the one side of the magnet holder to translate the magnet holder and prism holder, and furthermore to shift the laser beam. Figure 3(b) refers to one translational VCM actuation. In summary, the proposed 4-DOF FSM consists of two rotational VCMs and two translational VCMs so the proposed 4-DOF FSM has 4-DOF movements in total.

Journal Pre-proof

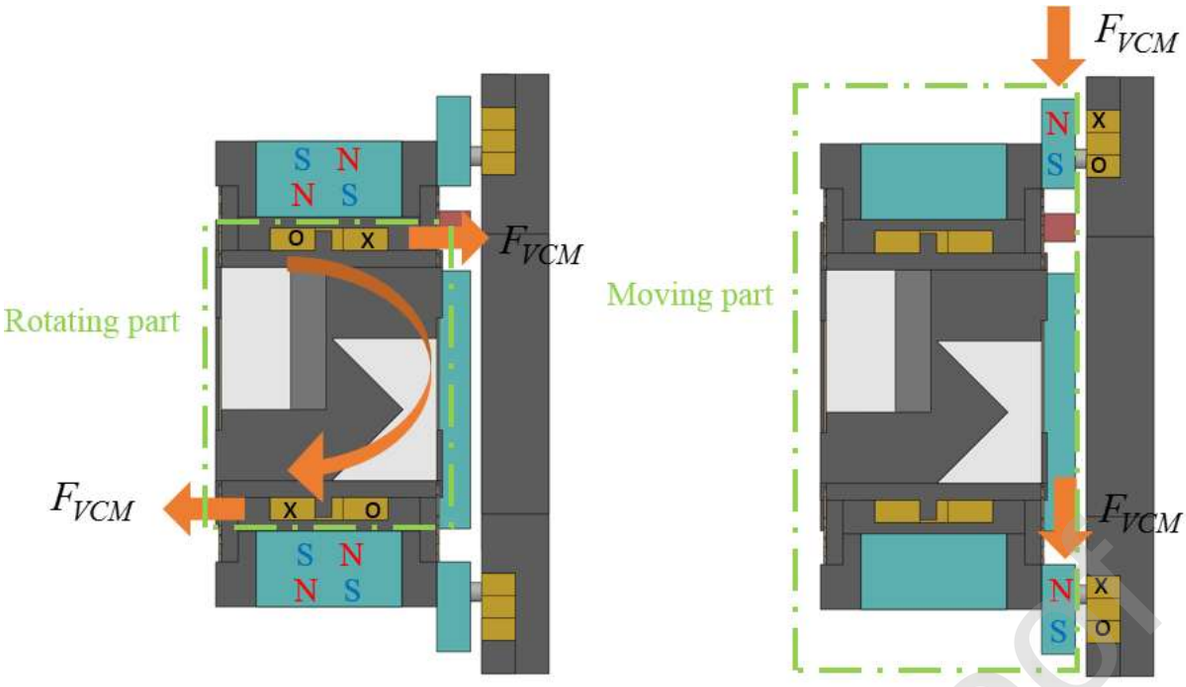


(a) (b)

Figure 3. Working principle of the proposed 4-DOF FSM: (a) rotational motion and (b) translational motion4-DOF.

## 3. Mathematical modeling of proposed 4-DOF FSM

In order to preliminary estimate the performance and shorten the design process of the proposed 4-DOF FSM, analytical modeling is indispensable. The proposed 4-DOF FSM could be considered to have a rotational part and a translational part. Both rotational motion and translational motion are assumed as ideal. There are no coupling issue between 4-DOF motions. The schematic models of the proposed 4-DOF FSM could be simplified as Fig. 4 (a) and Fig. 4 (b).

Fig. 4 (a) illustrates an ideal rotational model of the proposed 4-DOF FSM, where $I$ denotes the moment of inertia of the rotational part, $K_\theta$ denotes the torsional stiffness of spring plates, $c$ denotes the damping coefficient of spring plates and the rotational VCM, $l$ denotes the length between the rotational VCM and the center of the rotational part, $\theta$ denotes the rotational angle of the rotational part, $M$ denotes the torque generated by the rotational VCM. In this model, $\tan\theta \approx \theta$ is used since the rotational angle of the proposed 4-DOF FSM is quite small. According

Journal Pre-proof

to torque formula $T = I\alpha$ ($T$ denotes the torque and $\alpha$ denotes the angular acceleration), the rotational dynamic equation of the proposed 4-DOF FSM could be expressed as follows:

$$M - k_\theta \theta - cl^2 \dot{\theta} = I \ddot{\theta} \tag{1}$$

The electrical equation could be expressed as follows:

$$V - Ri - L\frac{di}{dt} = 0 \tag{2}$$

where $V$, $R$, $i$, and $L$ denote the input voltage, the resistance, the input current of VCM and the inductance of the rotational VCM, respectively.

The torque of the rotational VCM could be expressed as follows:

$$M = K_{VCM} il \tag{3}$$

where $K_{VCM}$ denotes the force coefficient of the rotational VCM.

The Laplace system transfer function could be expressed as follows through Eq. 1, Eq. 2 and Eq. 3:

$$G_s = \frac{\theta(s)}{V(s)} = \frac{2k_{VCM} l}{(Ls + R)\left(Is^2 + cl^2 s + K_\theta\right)} \tag{4}$$

As shown in Fig. 4 (b), $m$ denotes the mass of the translational part, $K$ denotes the stiffness of elastic strings, $c$ denotes the damping coefficient of elastic strings and the translational VCM, $x$ denotes the displacement of the translational part. According to force formula $F = ma$ ($F$ denotes the force and $a$ denotes the acceleration), the translational dynamic equation of double Porro Prisms FSM could be expressed as follows:

$$F - kx - c\dot{x} = m\ddot{x} \tag{5}$$

The electrical equation could be expressed as follows:

Journal Pre-proof

$$V - Ri - L\frac{di}{dt} = 0$$

(6)

The force of the translational VCM could be expressed as follows:

$$F = K_{VCM} i \tag{7}$$

The Laplace system transfer function could be expressed as follows through Eq. 1 and Eq. 2:

$$G_s = \frac{x(s)}{V(s)} = \frac{2k_{VCM}}{(Ls+R)\left(ms^2 + cs + K\right)} \tag{8}$$

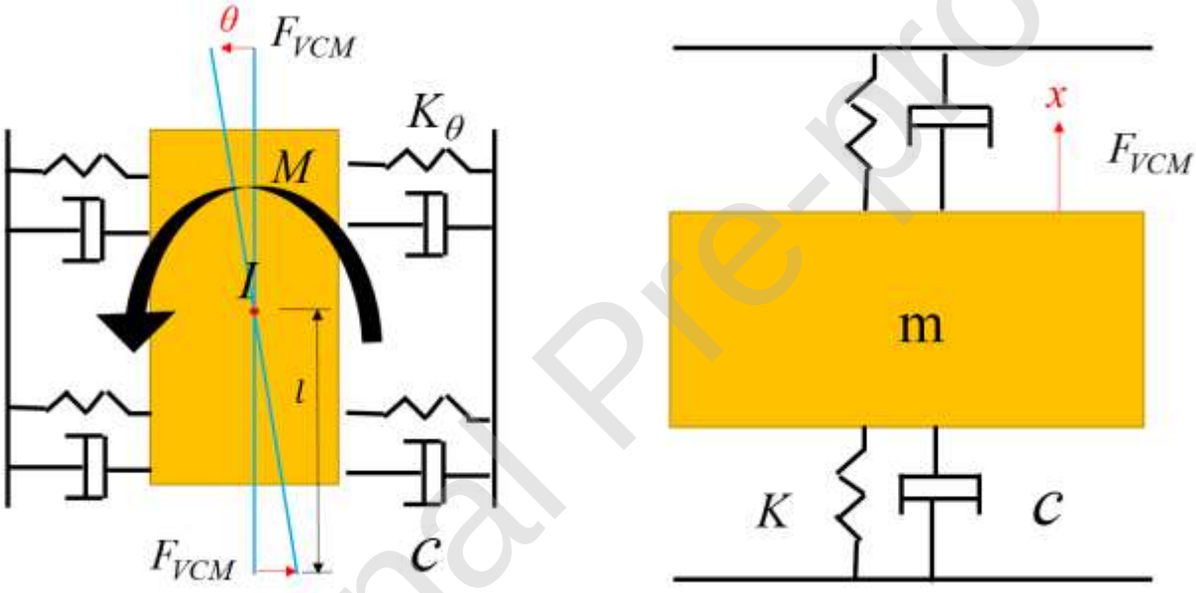


(a) (b)

Figure 4. Schematic model of proposed 4-DOF FSM: (a) rotational model and (b) translational model.

The dynamic simulation result are shown in Chapter 5 to compare experiment result.

## 4. Simulation of electromagnetic and mechanical structure

In this section, finite element analysis (FEA) was performed using commercial software Magnet and ANSYS to analyze the characteristics of the proposed electromagnetic and mechanical structure.

Journal Pre-proof

## 4.1 Simulation of electromagnetic structure

Table 1 shows the design parameters of the proposed electromagnetic structure. Figs. 5(a) and 5(b) illustrate the calculated magnetic flux distributions and magnetic force lines in the rotational VCM and translational VCM of the proposed 4-DOF FSM. The rotational VCMs along single axis consist two independent and opposite-direction VCMs, and Fig. 5(a) shows only one of the rotational VCMs. As shown, the magnet is horizontal magnetized and the coil is set at lateral side of the magnet to make the densest magnetic force lines pass two cross sections of the coil. Moreover, the simulation results show that the $K_{VCM}$ = 2.88 N-m/A. Also, the translational VCMs along single axis consist two independent and same-direction VCMs, and Fig. 5(b) shows only one of the translational VCMs. As shown, the magnet is perpendicular magnetized and the coil is set at bottom side of the magnet to make the densest magnetic force lines pass two cross sections of the coil. Moreover, the simulation results show that the $K_{VCM}$ = 1.5 N/A.

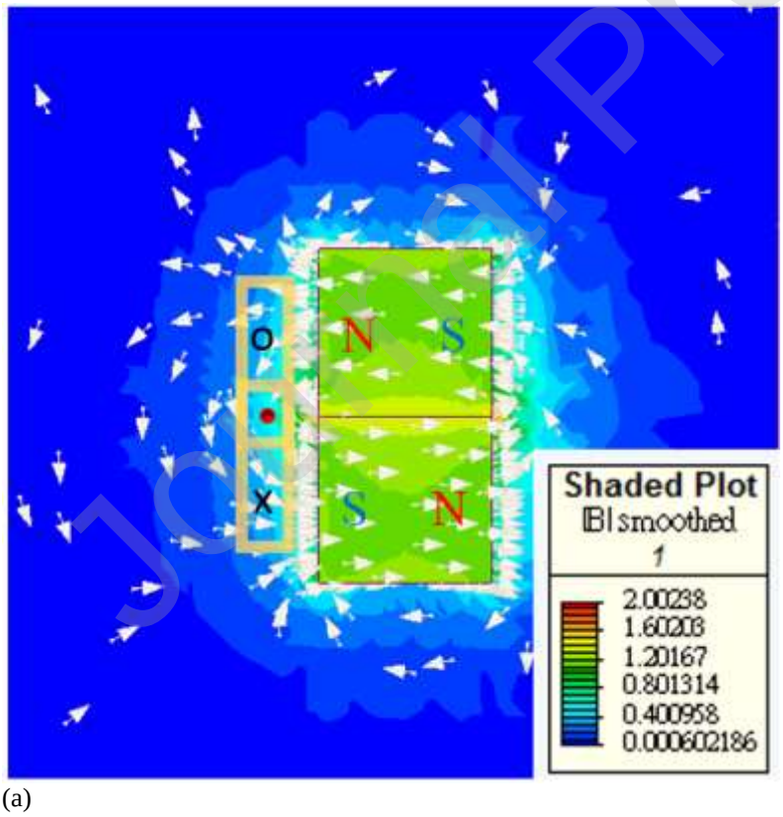


(a)

Journal Pre-proof

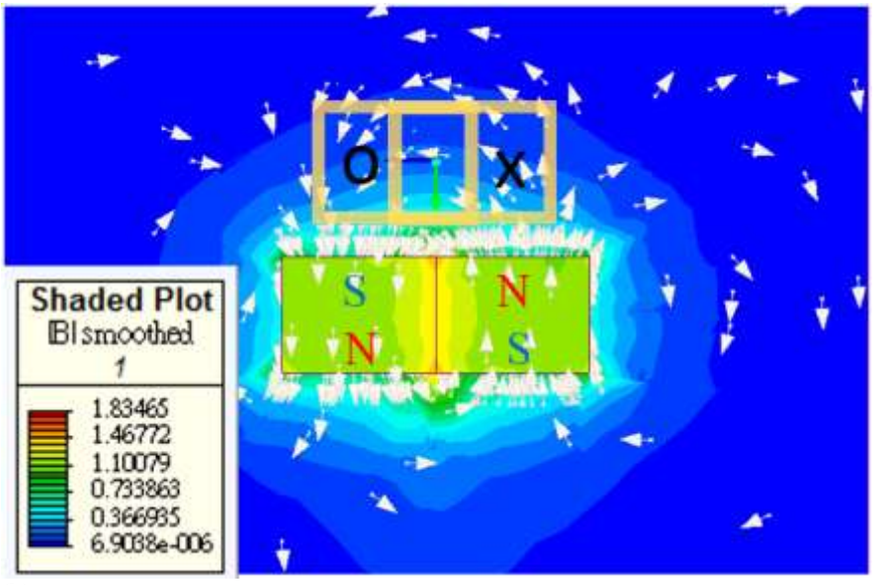


(b)

Figure 5. Distributions of magnetic flux: (a) rotational VCM and (b) translational VCM of proposed 4-DOF FSM.

Table 1. Design parameters of proposed electromagnetic structure.

| | Variable | Corresponding value |
|---|---|---|
| Rotational magnet | $(BH)_{max}$ (MGOe)<br>Material<br>Dimensions (mm) | 43-46<br>NdFeB N46H<br>44.1×26×13.5 |
| Translational magnet | (BH) max (MGOe)<br>Material<br>Dimensions (mm) | 43-46<br>NdFeB N46H<br>6×46×16 |
| Rotational coil | Outer dimensions (mm)<br>Cross-sectional area (mm) | 21×40×4<br>4×8 |
| Translational coil | Outer dimensions (mm)<br>Cross-sectional area (mm) | 12×53.7×6<br>4×6 |

## 4.2 Simulation of mechanical structure

In the proposed mechanical structure, spring plates and elastic strings are utilized to suspend the double Porro prisms and balance the torque and force of the VCMs. Furthermore, the torsional stiffness of spring plates and the translational stiffness of elastic strings are directly related to the travel range and dynamic performance of the proposed 4-DOF FSM. Note that the elastic string is assumed to be a fixed-pinned beam to best reflect the practical boundary conditions. Table 2 shows the design parameters of mechanical structure. Figs. 6(a) and 6(b) illustrate the simulation results

Journal Pre-proof

for the von Mises stresses of the spring plates and the elastic string, respectively. The simulation results show that the stress values of spring plates and elastic string at motional direction are both under the yield stresses of the materials which means the proposed 4-DOF FSM will not break or have permanent deformation under normal operation and could keep a gap in VCMs to avoid interference. It is noted that the torsional stiffness of spring plates $K_\theta$ and the stiffness of elastic strings $K$ are 46.6 N-m/rad and 4110 N/m, respectively.

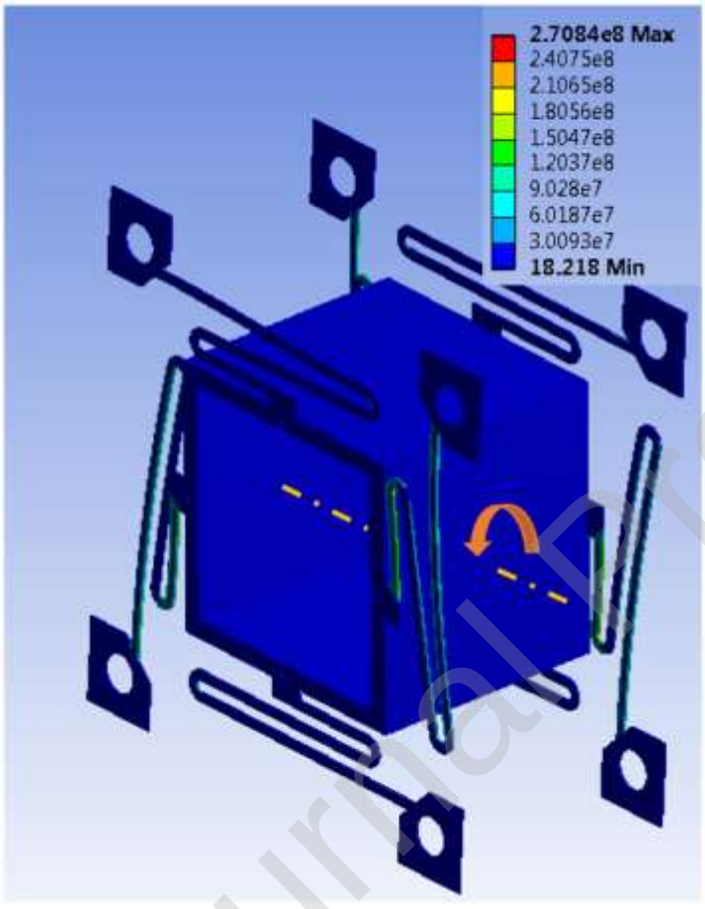


(a)

Journal Pre-proof

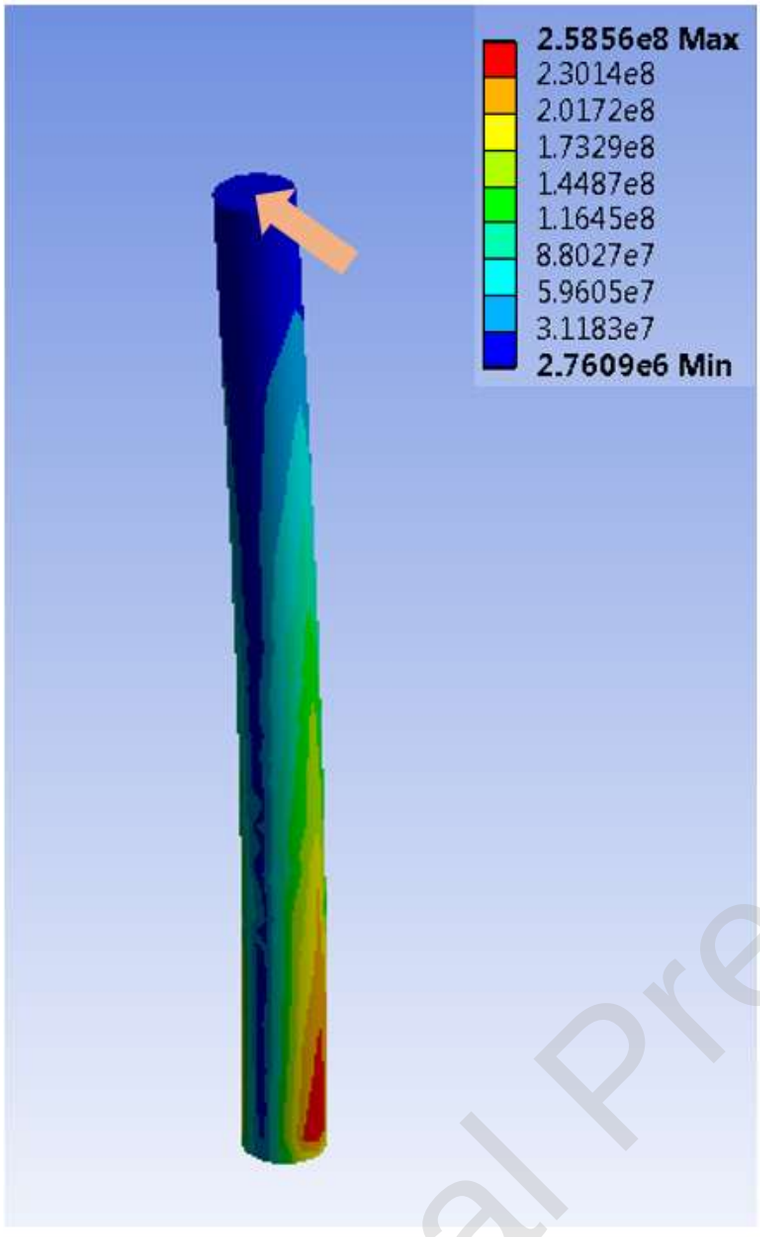


(b)

Figure 6. (a) von Mises stresses of spring plates (rotational angle of 10 mrad) (b) von Mises stresses of elastic string (translation of 1mm).

Table 2. Design parameters of mechanical structure.

| Variable | Spring plate | Elastic string |
|---|---|---|
| Material | C17200 copper | Ti4Al22V |
| Elastic modulus (GPa) | 125 | 97 |
| Yield stress (Mpa) | 1205 | 1154 |
| Tensile stress, Ultimate (Mpa) | 1480 | 1235 |
| Dimensions (mm) | 83.1×83.1×0.4 | Φ=2.2, Length=43.4 |

Journal Pre-proof

## 5. Performance verification of proposed 4-DOF FSM

In this section, a laboratory-built prototype was built to evaluate the performance of the proposed 4-DOF FSM. Fig.7 shows the angular measurement setup. As shown, the experiment involves the use of a He-Ne laser (EL01A, 632 nm, 10 mW, LASOS), a beam splitter (BS) and a dual-axis lateral position-sensitive diodes (PSD) (SPOTANA-9S-USB-L, DUMA OPTRONICS), a proposed prototype. The laser source incidents through the BS to the mirror which is stuck on the prototype, and then is reflected back to the BS. Finally, the laser beam is reflected into the PSD. When the prototype is actuated, the rotation of the mirror makes the reading of the PSD change. Therefore, the rotational angle of the prototype could be calculated by trigonometric principle when the reading of the PSD and the optical length between the mirror and the PSD are known. Fig. 8 shows the displacement measurement setup. As shown, a laser displacement meter (Keyence LK-G80) is utilized to measure the displacement of the prototype. The prototype is set at a measurable distance beside the displacement meter. When the prototype is actuated, the displacement meter could measure the displacement.

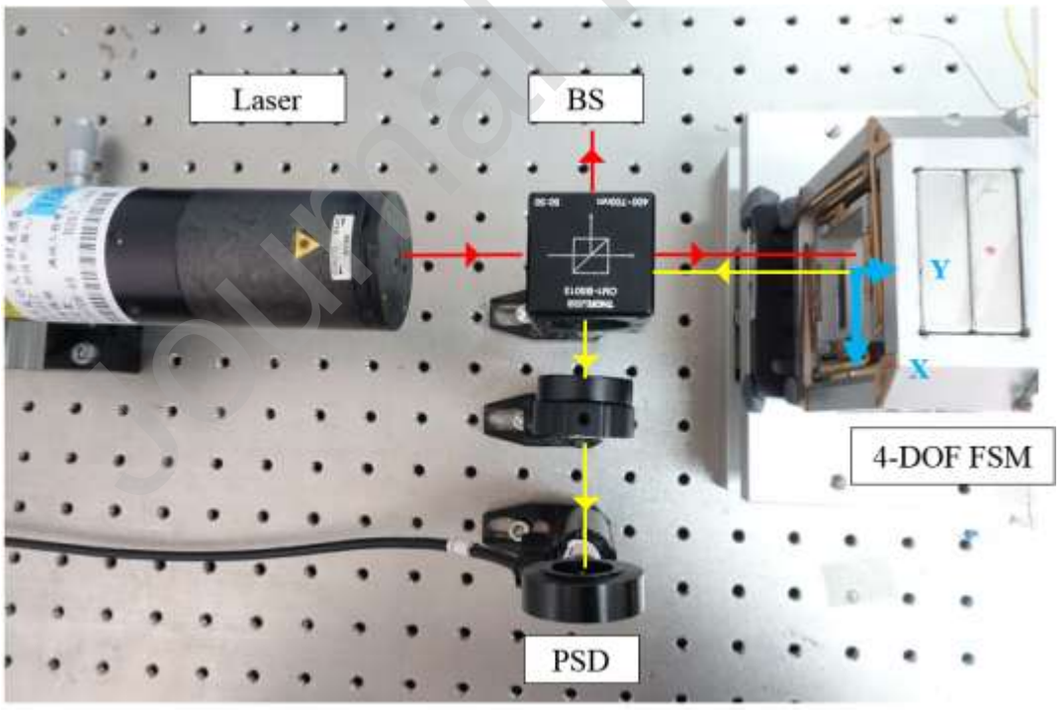

Figure 7. Experimental setup of angular measurement.

Journal Pre-proof

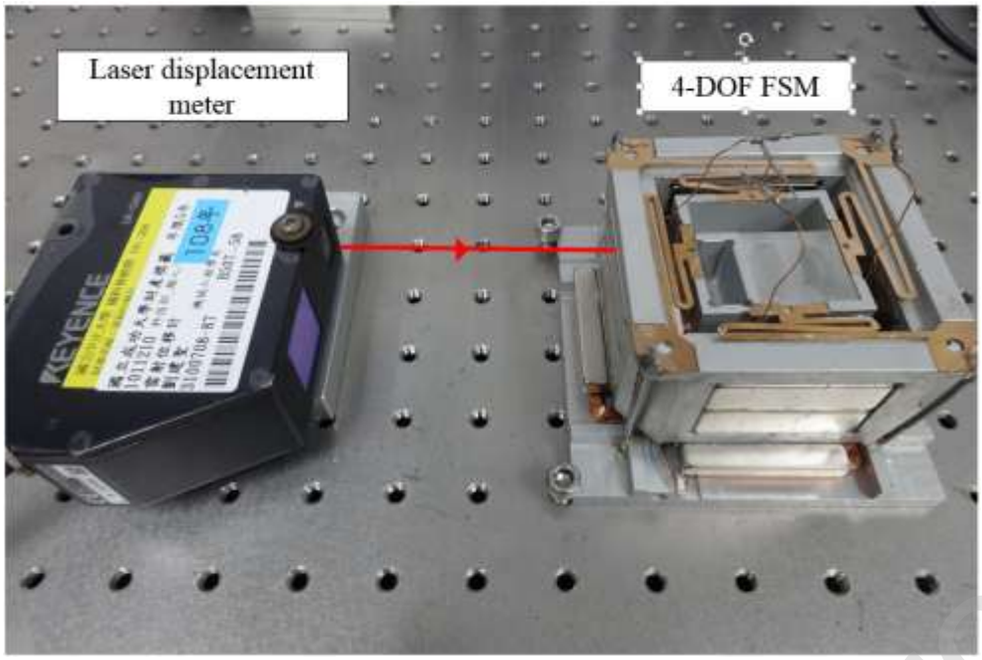

Figure 8. Experimental setup of displacement measurement.

Figs. 9(a) and 9(b) show the angular measurement results of the prototype along X and Y axes, respectively. As shown, the rotational movement of the prototype along X and Y axes have similar results. The rotational movement of the prototype has a linear output curve and ±5 mrad stroke. Figs. 10(a) and 10(b) show the translational measurement results of the prototype along X and Y axes, respectively. As shown, the translational movement of the prototype along X and Y axes have similar results. The translational movement of the prototype has a linear output curve and ±0.04 mm stroke.

Journal Pre-proof

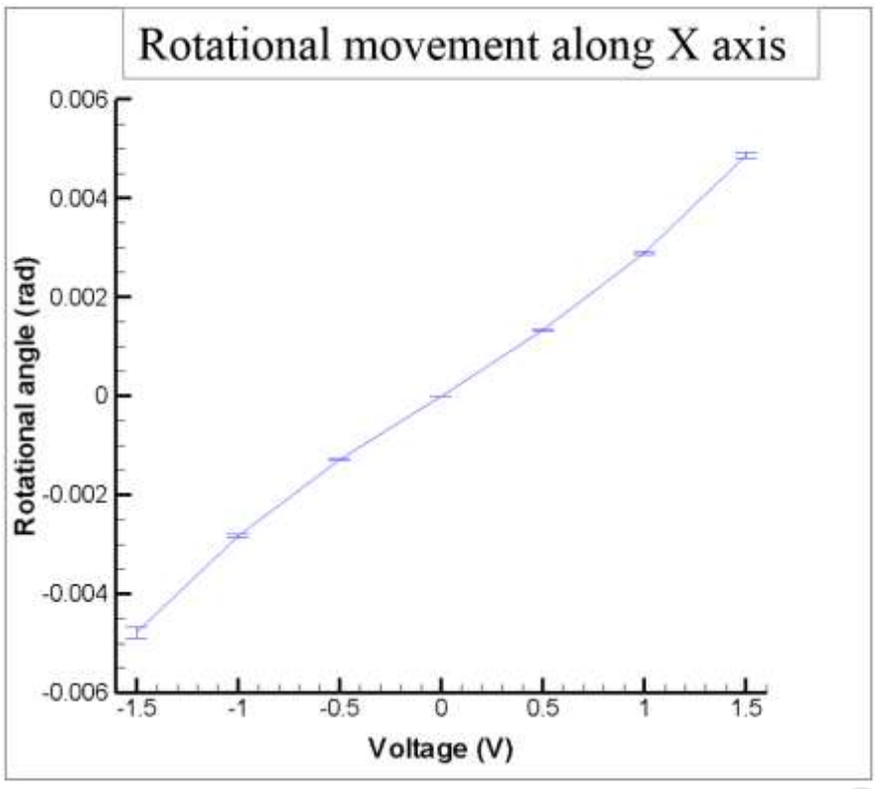


(a)

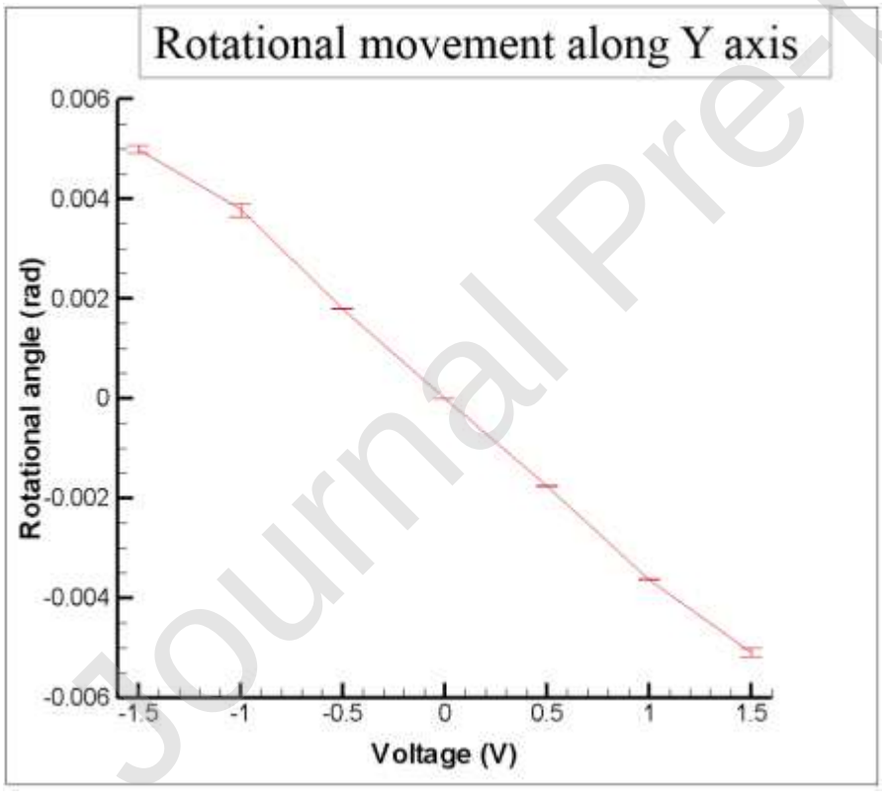


(b)

Figure 9. Angular performance of prototype under various voltage (a) rotational movement along X axis (b) rotational movement along Y axis.

Journal Pre-proof

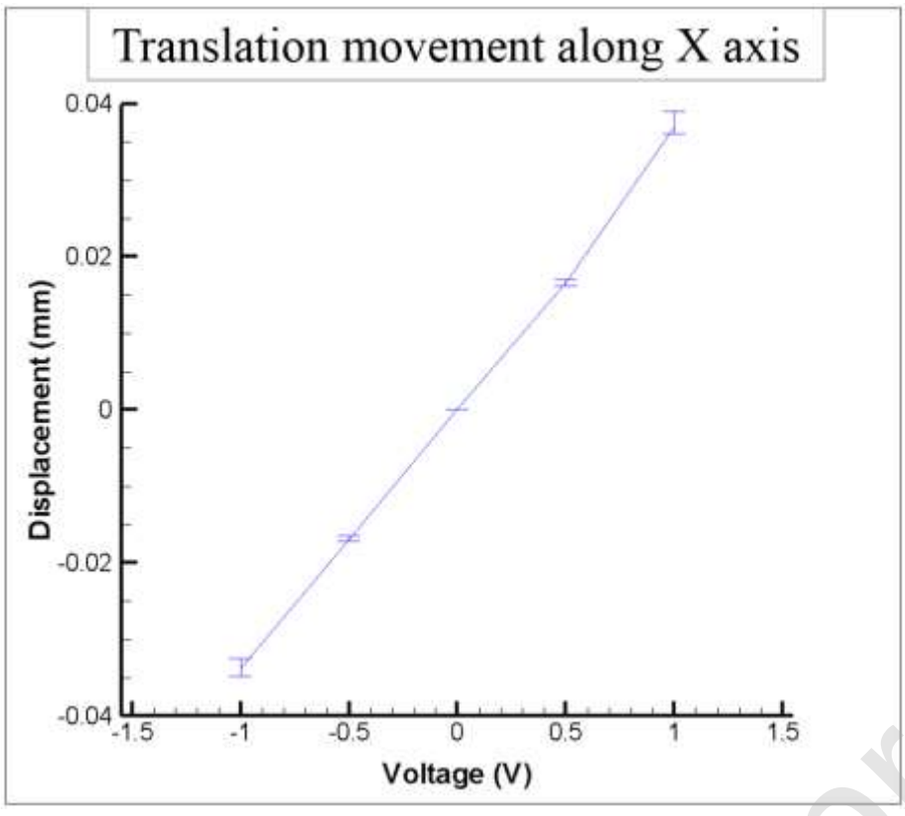


(a)

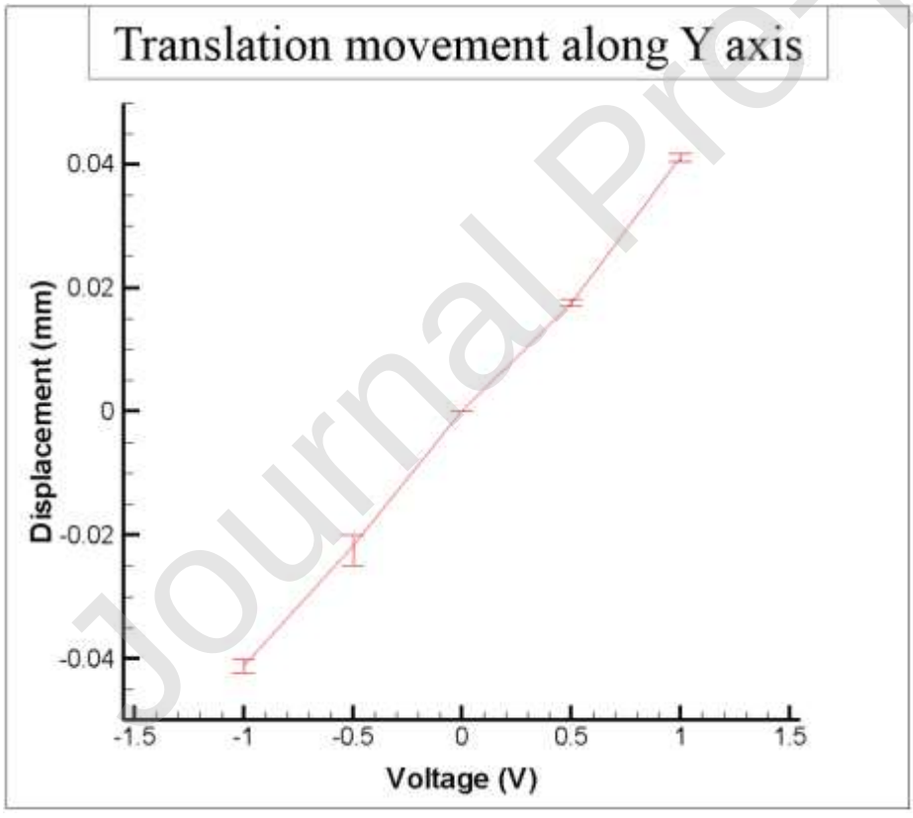


(b)

Figure 10. Translational performance of prototype under various voltage (a) translational movement along X axis (b) translational movement along Y axis.

Journal Pre-proof

The modeling parameters of the proposed 4-DOF FSM are listed in Table 3. The parameters of $I$ and $m$ are designed and automatically obtained by 3D CAD software (SolidWork), the parameters of $K_\theta$ and $K$ are obtained by FEA software (Ansys) and the parameters of $K_{VCM}$ and $L$ are obtained by FEA software (Magnet). In Table 3, $K_1$ denotes the correction factor of modeling. Figures 11 and 12 show the dynamic response performance of rotational part and translational part of the proposed 4-DOF FSM, respectively. Figure 11 shows the Bode diagram of modeling result and experimental result for the rotational motion. It is noted that there is an oscillating curve before resonance peak in the experimental Bode diagram. We can infer that the oscillating curve before peak is caused by manual sticking spring plates (the spring plate is not a 0.4mm thick plate; it is obtained by manually sticking four 0.1mm plates together for lowering the experimental cost). Therefore, if we can cooperate with companies to solve the producing problem, there will be no oscillating curve before peak. As shown in Figure. 12, the modeling result of the translational motion is close to the experimental result.

Table 3. Modeling parameters of proposed 4-DOF FSM.

| Rotational part | | Translational part | |
|---|---|---|---|
| Parameter | Value | Parameter | Value |
| $I$ (Kg·mm$^2$) | 0.0000536 | $m$ (kg) | 0.64 |
| $K_\theta$ (N·m/rad) | $46.6\times K_1$ | $K$ (N·m) | 4110 |
| $c$ (N·s/m) | 20 | $c$ (N·s/m) | 59.6 |
| $l$ (mm) | 0.026 | $K_{VCM}$ (N/A) | 1.35 |
| $K_{VCM}$ (N/A) | 2.88 | $R$ ($\Omega$) | 2.48 |
| $R$ ($\Omega$) | 1.29 | $L$ (H) | 0.0013 |
| $L$ (H) | 0.0014 | | |
| Volume of single 90° prism (mm$^3$) | 7968 | | |

Journal Pre-proof

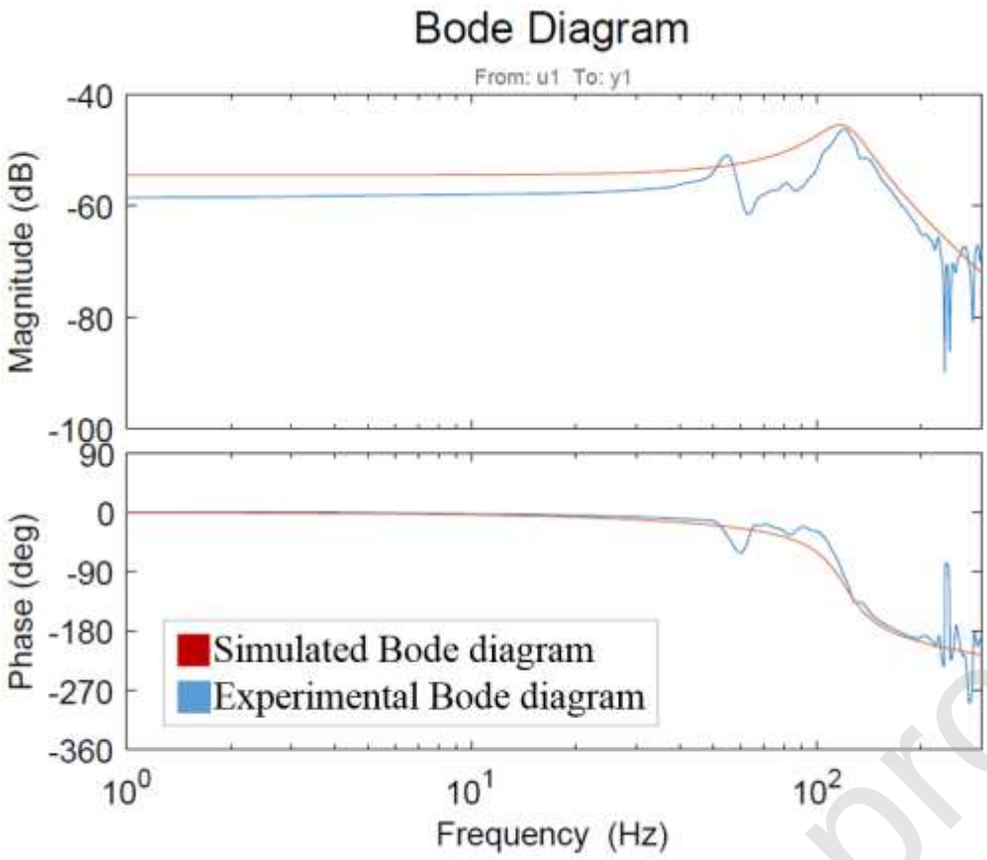


Figure 11. Open-loop dynamic response performance of rotational part

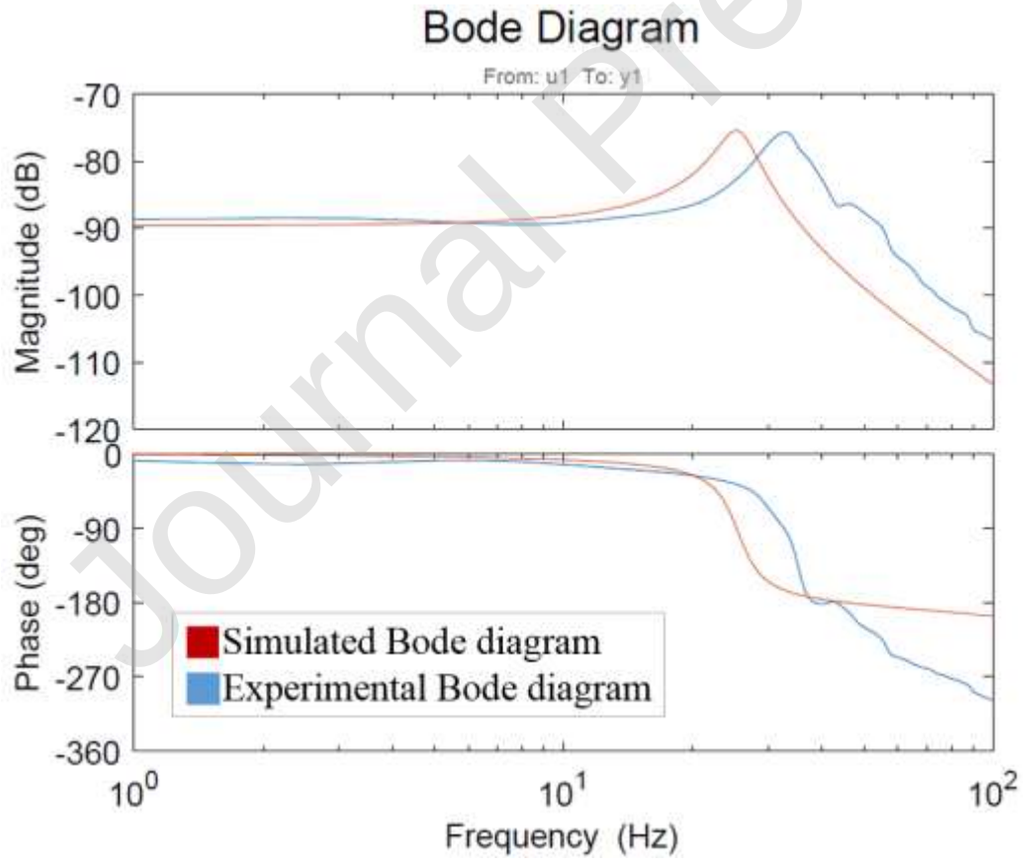


Figure 12. Open-loop dynamic response performance of translational part

Journal Pre-proof

## 6. Laser error compensation of proposed 4-DOF FSM

This section will focus on the verification of the proposed 4-DOF FSM compensation system. In our previous research [29], screw-ray tracing method was utilized to analyze the 4-DOF laser errors and compute the compensation command. However, there are several defects of using screw-ray tracing method in FSM compensation systems. The model built by screw-ray tracing method is an ideal system model, however the experimental optical setup involves assembly errors. So the system model built by screw-ray tracing method is difficult to analyze the accurate 4-DOF laser errors, and compensate the laser errors completely. In addition, it is a large amount of calculation that utilized screw-ray tracing method to solve 4-DOF laser errors and compute the compensation command. It is not suitable for instant compensation. This study utilized another method to compensate 4-DOF laser errors. As shown in Fig. 13, there is a focusing lens which is set in front of the PSD 2. The distance between the focusing lens and PSD 2 is the focusing length of the focusing lens. Using this setting, only laser beam's angular errors will cause the light spot move on the PSD 2, translational errors will not [14]. PSD 2 only reads two angular laser errors and PSD1 read both two angular laser errors and two translational laser errors. So as long as zero the value of the light spot on PSD 2, then zero the value of the light spot on PSD 1 (translational laser errors left only), and finally the 4-DOF laser errors are compensated.

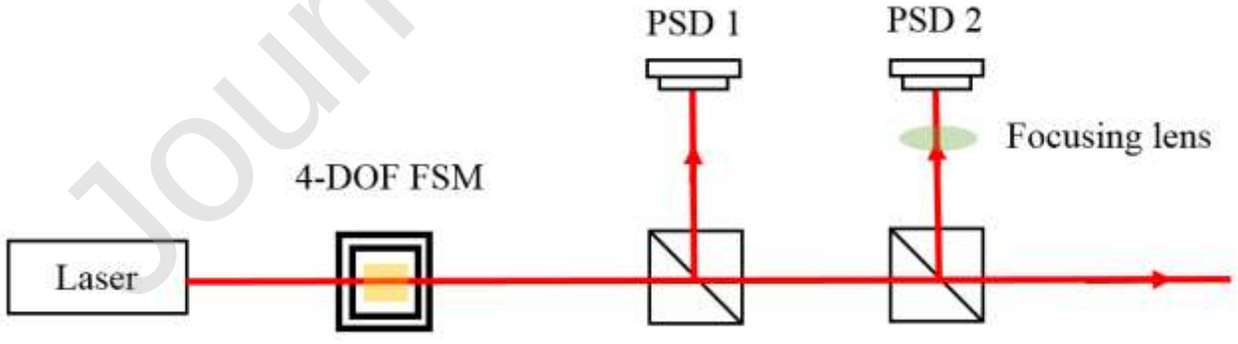


Figure 13 Experiment setup of 4-DOF FSM compensation.

As shown in Fig. 14, the prototype of the proposed 4-DOF FSM compensation system is set on the optical bench. This compensation system includes the use of a He-Ne laser (EL01A, 632

Journal Pre-proof

nm, 10 mW), a 2-axis translation stage, a mirror, a 2-axis rotation stage, a 4-DOF FSM, two BSs, a focusing lens and two dual-axis lateral PSDs (SPOTANA-9S-USB-L). The He-Ne laser is used as the light source, which is set on the 2-axis linear translation stage. The mirror is set on a 2-axis rotation stage.

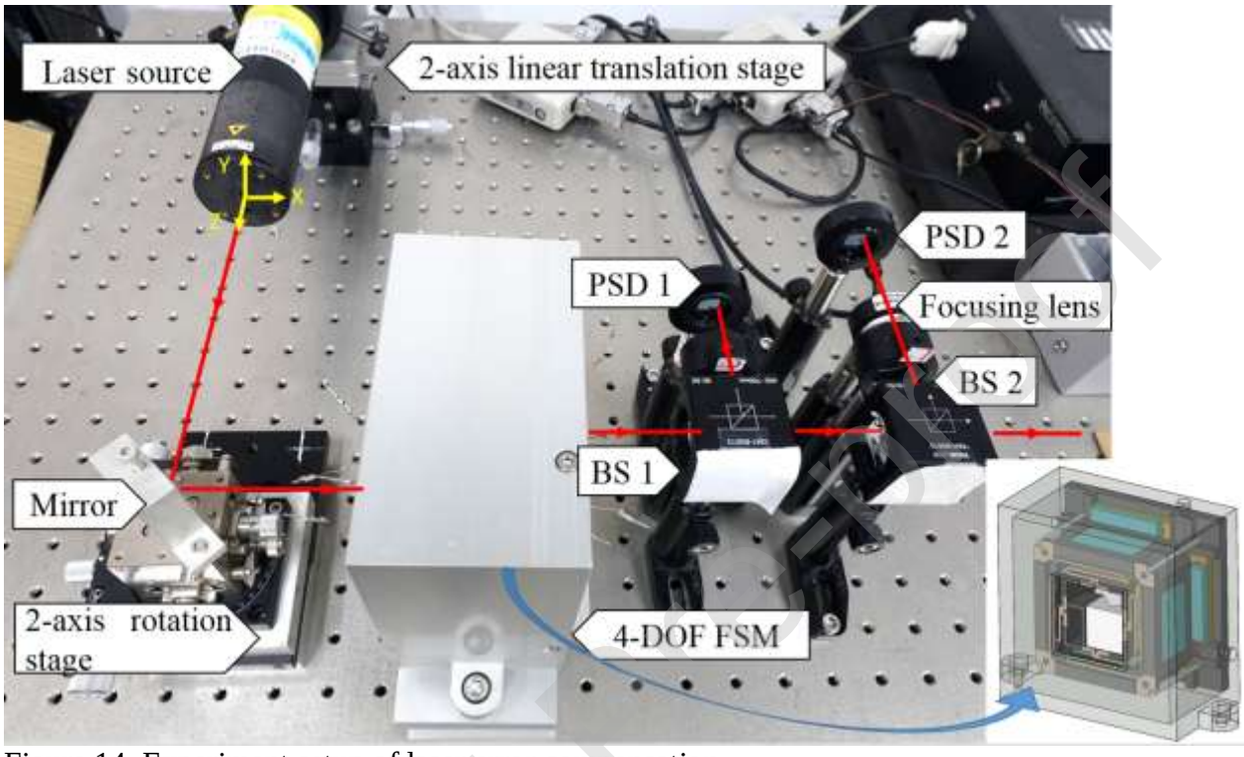


Figure 14. Experiment setup of laser error compensation.

The laser beam incidents to the mirror, then reflects to the 4-DOF FSM, and is then directed into the BS 1. Then the laser beam is split into the PSD 1 and the BS 2 by the BS 1. Finally, the laser beam split through the focusing lens into the PSD 2 by the BS 2. The 2-axis linear translation stage and 2-axis rotation stage are applied to produce 2-DOF translational errors along x axis and y axis (namely $\delta_x$ and $\delta_y$) and 2-DOF rotational errors along x axis and y axis (namely $\theta_x$ and $\theta_y$).

The experiments below will compensate 4-DOF laser errors separately. Figs. 15(a) and 15(b) show the experimental results for the variation of positions of light spots on the PSDs with and without the compensation, when the laser error is $\delta_x$ = 20 μm and $\delta_x$ = −20 μm, respectively. As shown in Fig. 15(a), the readings of the PSD 1 and PSD 2 are -20 and 0 μm when $\delta_x$ = 20 μm

Journal Pre-proof

(PSD2 read angular laser errors only). After compensating for the laser error, the readings of the PSD 1 and the PSD 2 are reduced to approximately 0 μm, which means that the laser error of $\delta_x$ = 20 μm is compensated by the proposed FSM compensation system. The same is seen in Fig. 15(b), where the result shows that the readings of two PSDs are reduced to around 0 μm, which means that the laser error of $\delta_x = -20$ μm is compensated by the proposed FSM compensation system. Figs. 16(a) and 16(b) show the experimental results for the variation of positions of light spots on the PSDs with and without the compensation, when the laser error is $\delta_y = 20$ and $\delta_y = -20$ μm, respectively. As shown in Fig. 16(a), the readings of the PSD 1 and the PSD 2 are 20 and 0 μm when $\delta_y = 20$ μm. After compensating for the laser error, the readings of the PSD 1 and the PSD 2 are reduced to approximately 0 μm, which means that the laser error of $\delta_y = 20$ μm is compensated by the proposed FSM compensation system. The same is seen in Fig. 16(b), where the result shows that the readings of two PSDs are reduced to around 0 μm, which means that the laser error of $\delta_y = -20$ μm is compensated by the proposed FSM compensation system.

Figs. 17 and 18 show the experimental results for the variation of positions of light spots on the PSDs with 1st, 2nd and without the compensation. These experiments compensate first angular errors (1st compensation) but there is a translation of light spots on the PSD 1 after compensating angular errors. Therefore, it needs a 2nd compensation that translate double Porro prisms to clear the translation of light spots on the PSD1. As shown in Fig. 17(a), the readings of the PSD 1 and PSD 2 are -120 μm and -20 μm when $\theta_x = 2.5$ mrad. After 1st compensation for the laser error (zero the light spots on the PSD 2), the readings of PSD 1 and PSD 2 are reduced to approximately -55 and 0 μm, which means that the angular laser error is compensated but still a translation of light spots on the PSD 1. Then after 2nd compensation both the readings of PSD 1 and PSD 2 are reduced to around 0 μm, which means that the laser error of $\theta_x = 2.5$ mrad is compensated by the proposed FSM compensation system. The same is seen in Fig. 17(b), where the result shows that the readings of two PSD 1 and PSD 2 are reduced to around 55 μm and 0 μm by 1st compensation, then reduced

Journal Pre-proof

to around 0 μm by 2nd compensation, which means that the laser error of $\theta_x = -2.5$ mrad is compensated by the proposed FSM compensation system.

As shown in Fig. 18(a), the readings of PSD 1 and PSD 2 are 120 μm and 20 μm when $\theta_y$ = 2.5 mrad. After 1st compensation for the laser error (zero the light spots on the PSD 2), the readings of the PSD 1 and the PSD 2 are reduced to approximately 50 μm and 0 μm, which means that the angular laser error is compensated but still a translation of light spots on the PSD 1. Then after 2nd compensation both the readings of PSD1 and PSD2 are reduced to around 0 μm, which means that the laser error of $\theta_y$ = 2.5 mrad is compensated by the proposed FSM compensation system. The same is seen in Fig. 18(b), where the result shows that the readings of two PSD 1 and PSD 2 are reduced to around -50 μm and 0 μm by 1st compensation, then reduced to around 0 μm by 2nd compensation, which means that the laser error of $\theta_y = -2.5$ mrad is compensated by the proposed FSM compensation system.

Journal Pre-proof

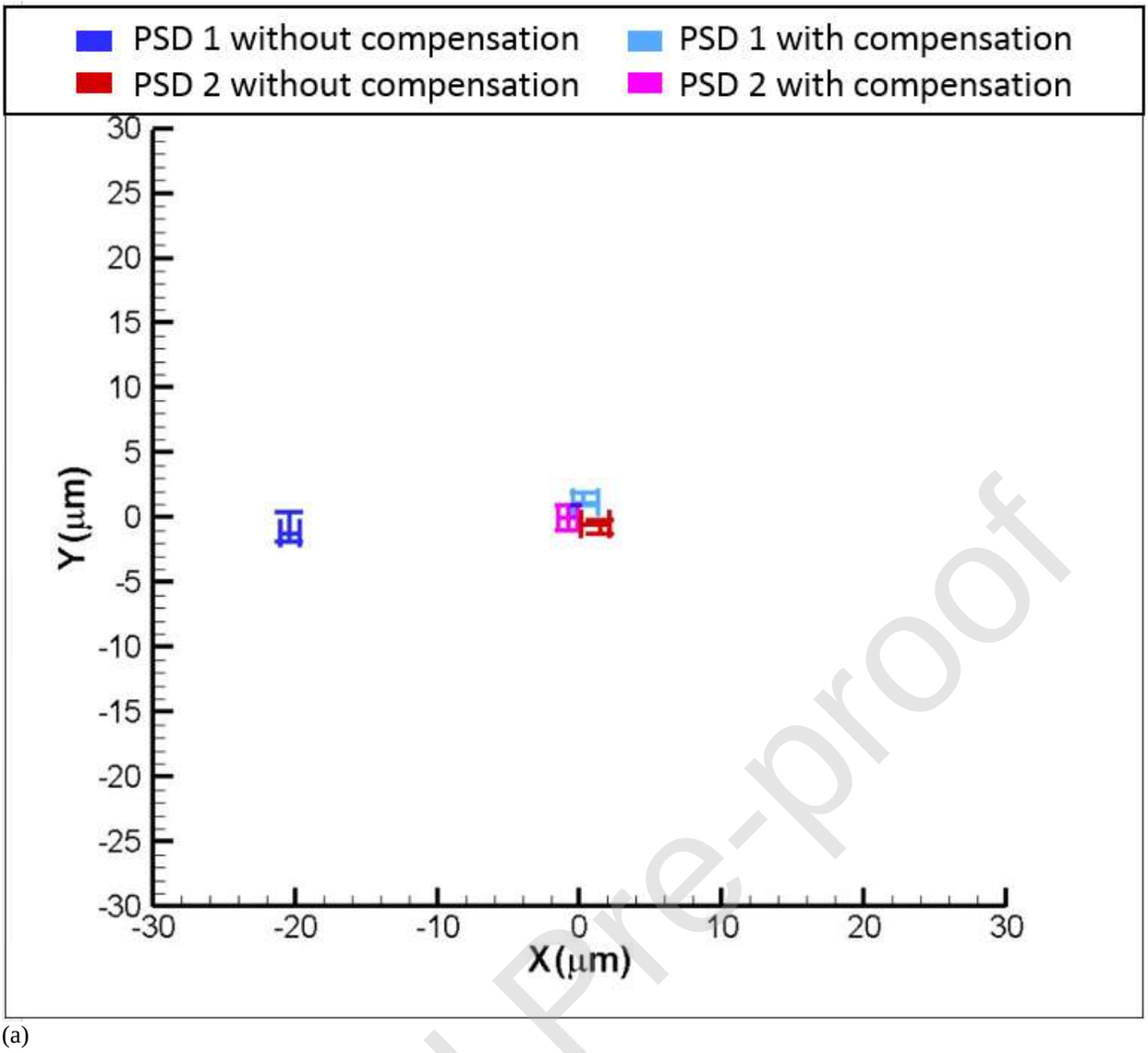


(a)

Journal Pre-proof

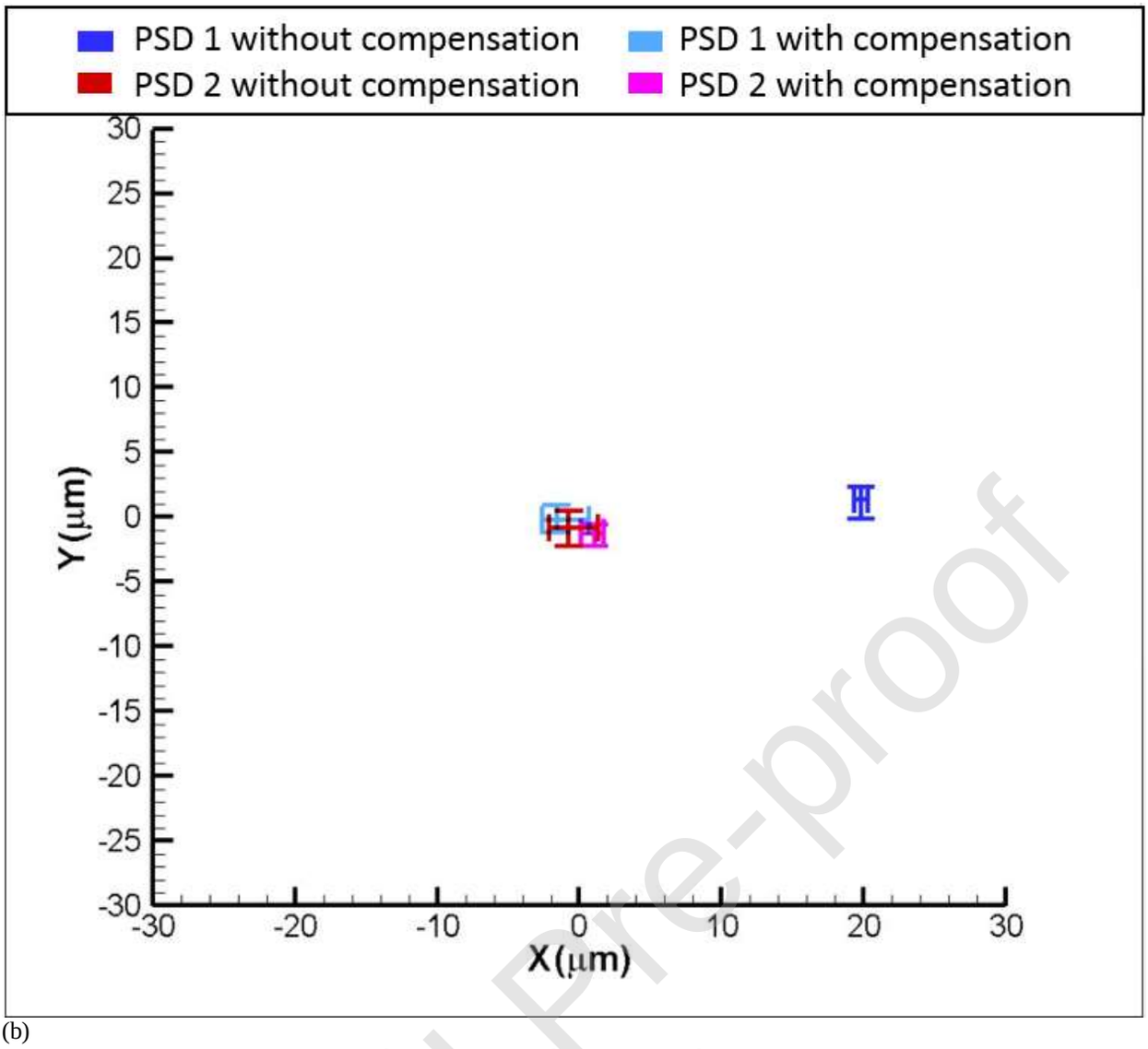


(b)

Figure 15. Experimental results for variation of positions of light spots on PSDs with and without compensation (a) $\delta_x$ = 20 μm and (b) $\delta_x$ = −20 μm, respectively.

Journal Pre-proof

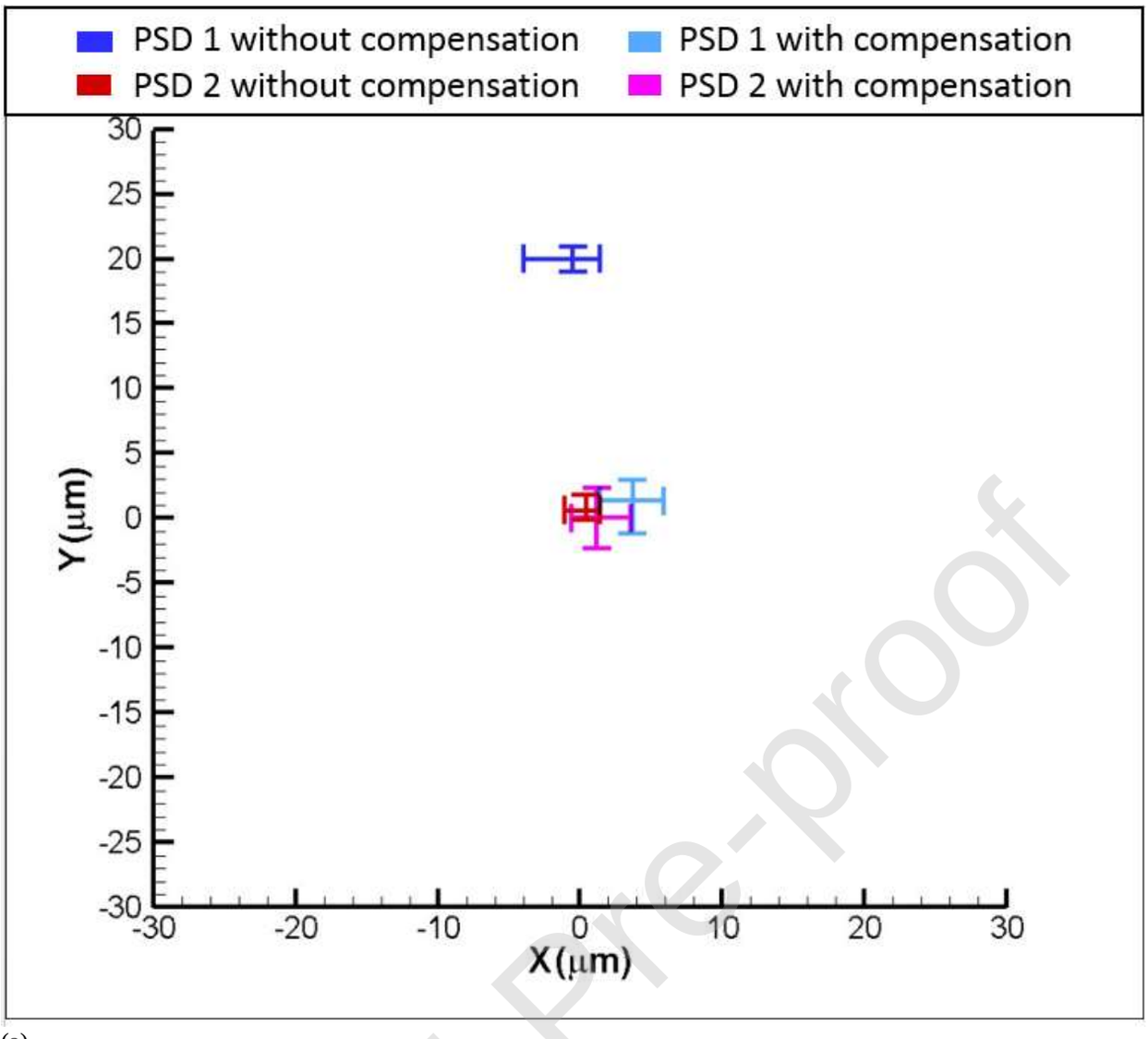


(a)

Journal Pre-proof

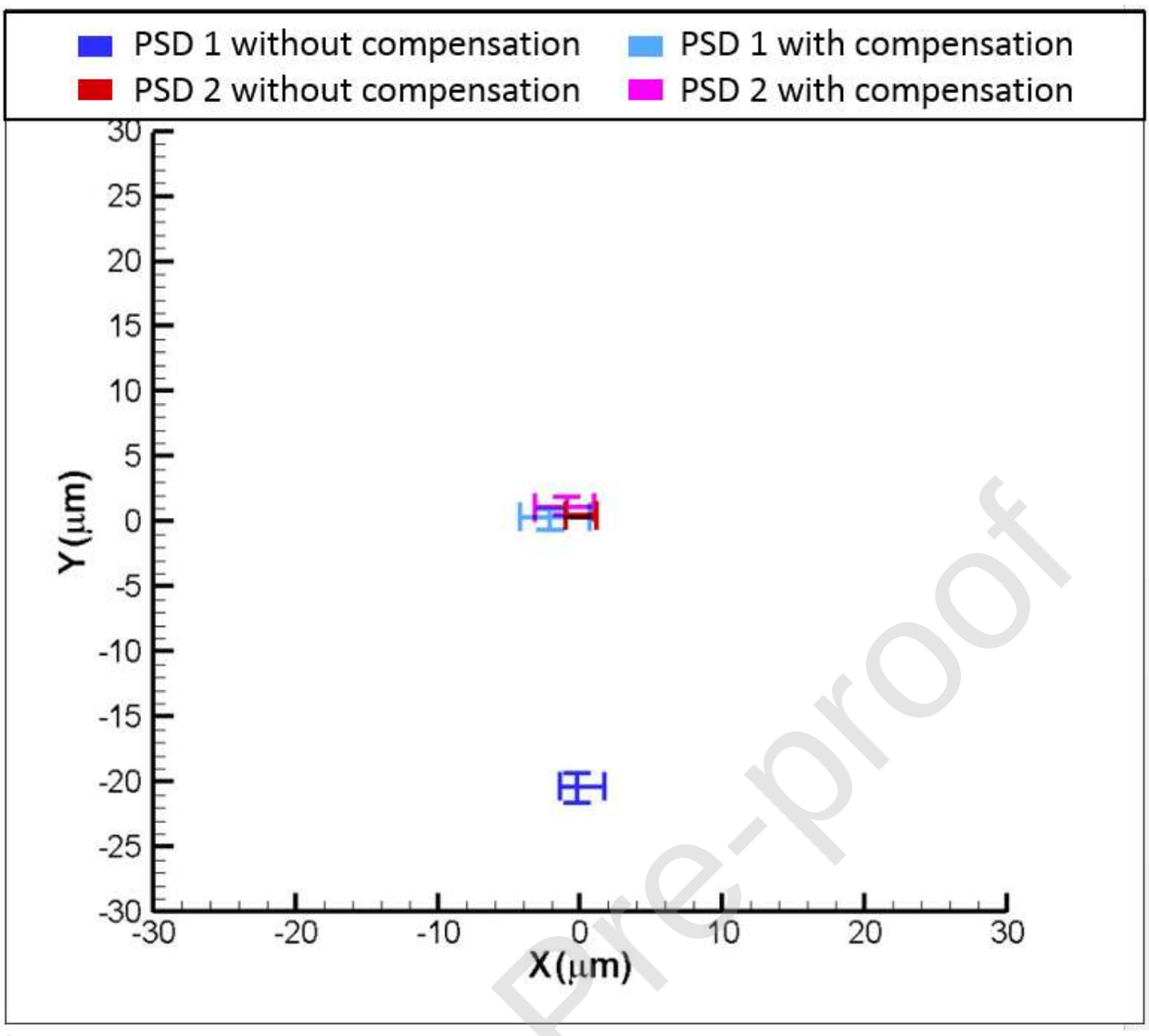


(b)

Figure 16. Experimental results for variation of positions of light spots on PSDs with and without compensation (a) $\delta_y = 20$ μm and (b) $\delta_y = -20$ μm, respectively.

Journal Pre-proof

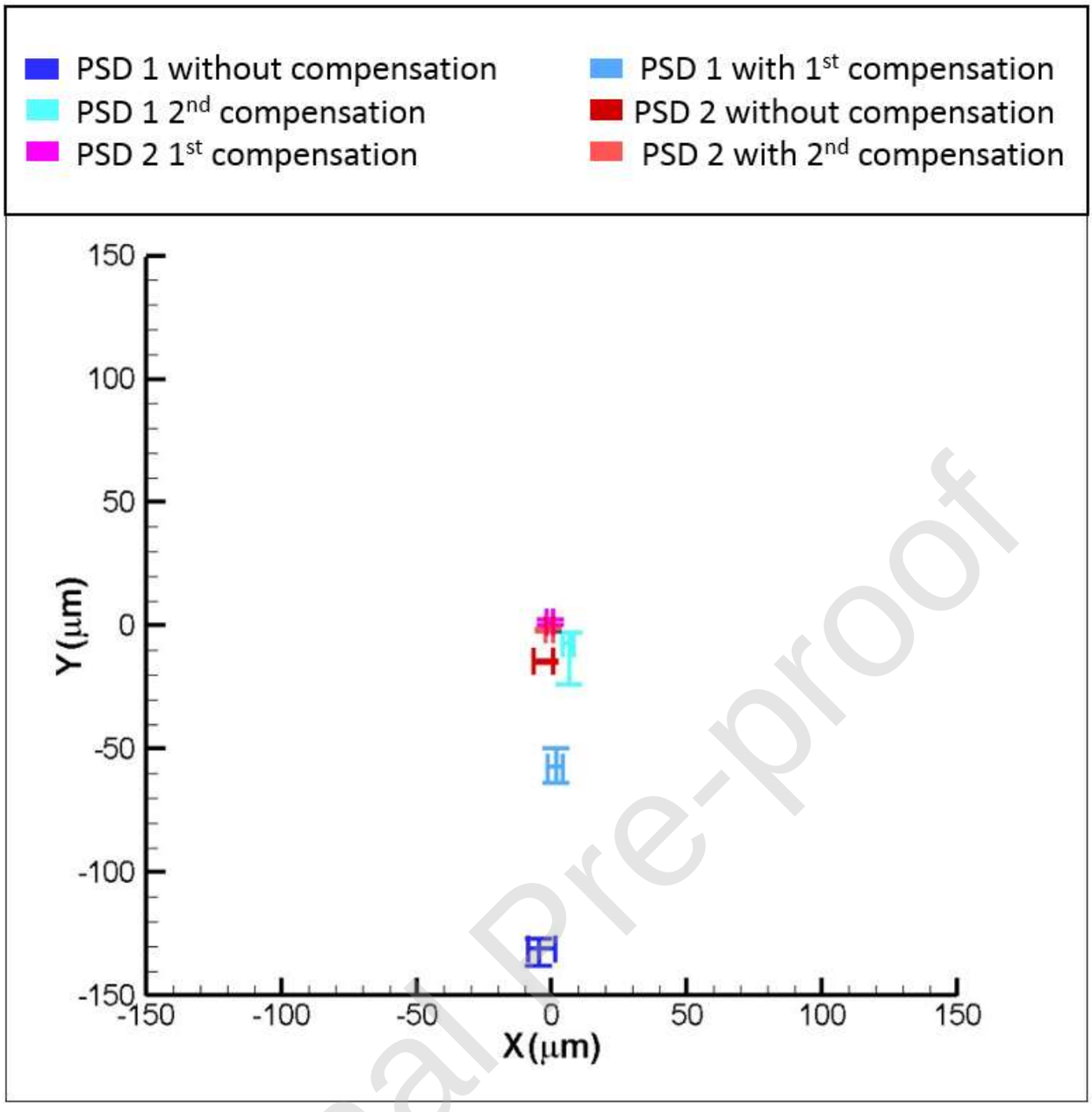


(a)

Journal Pre-proof

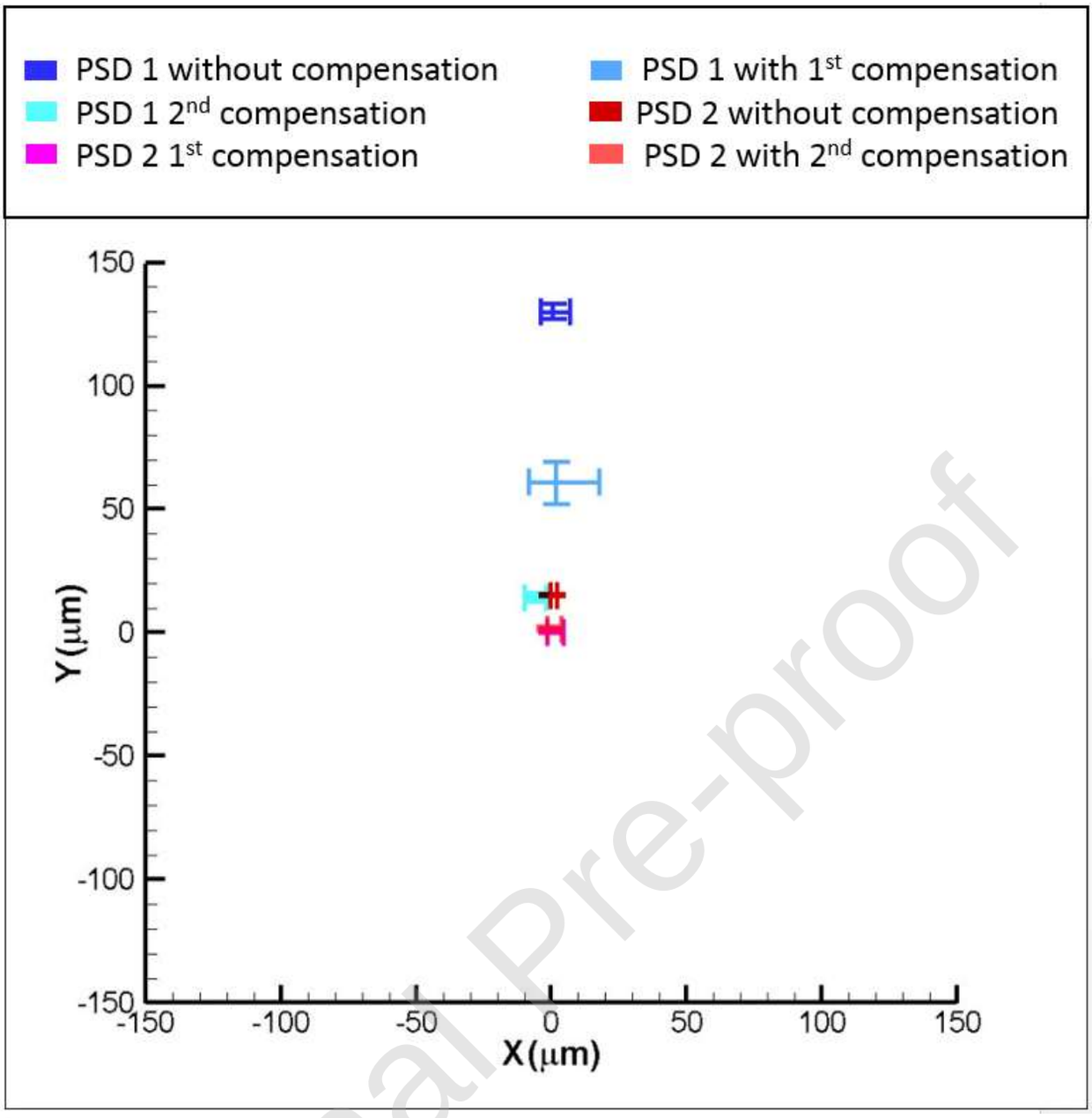


(b)

Figure 17. Experimental results for variation of positions of light spots on PSDs with and without compensation (a) $\theta_x$ = 2.5 mrad and (b) $\theta_x$ = −2.5 mrad, respectively.

Journal Pre-proof

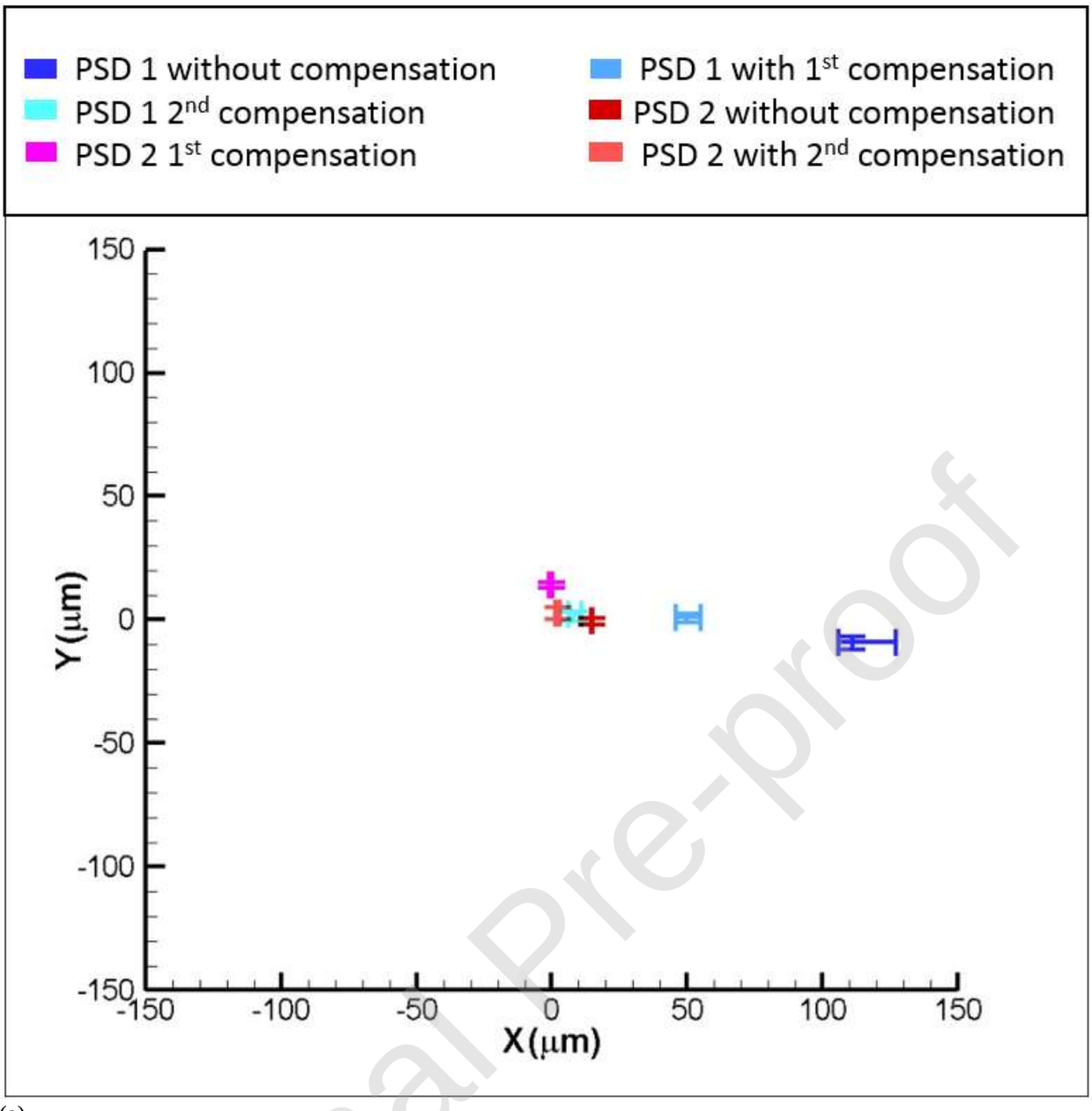


(a)

Journal Pre-proof

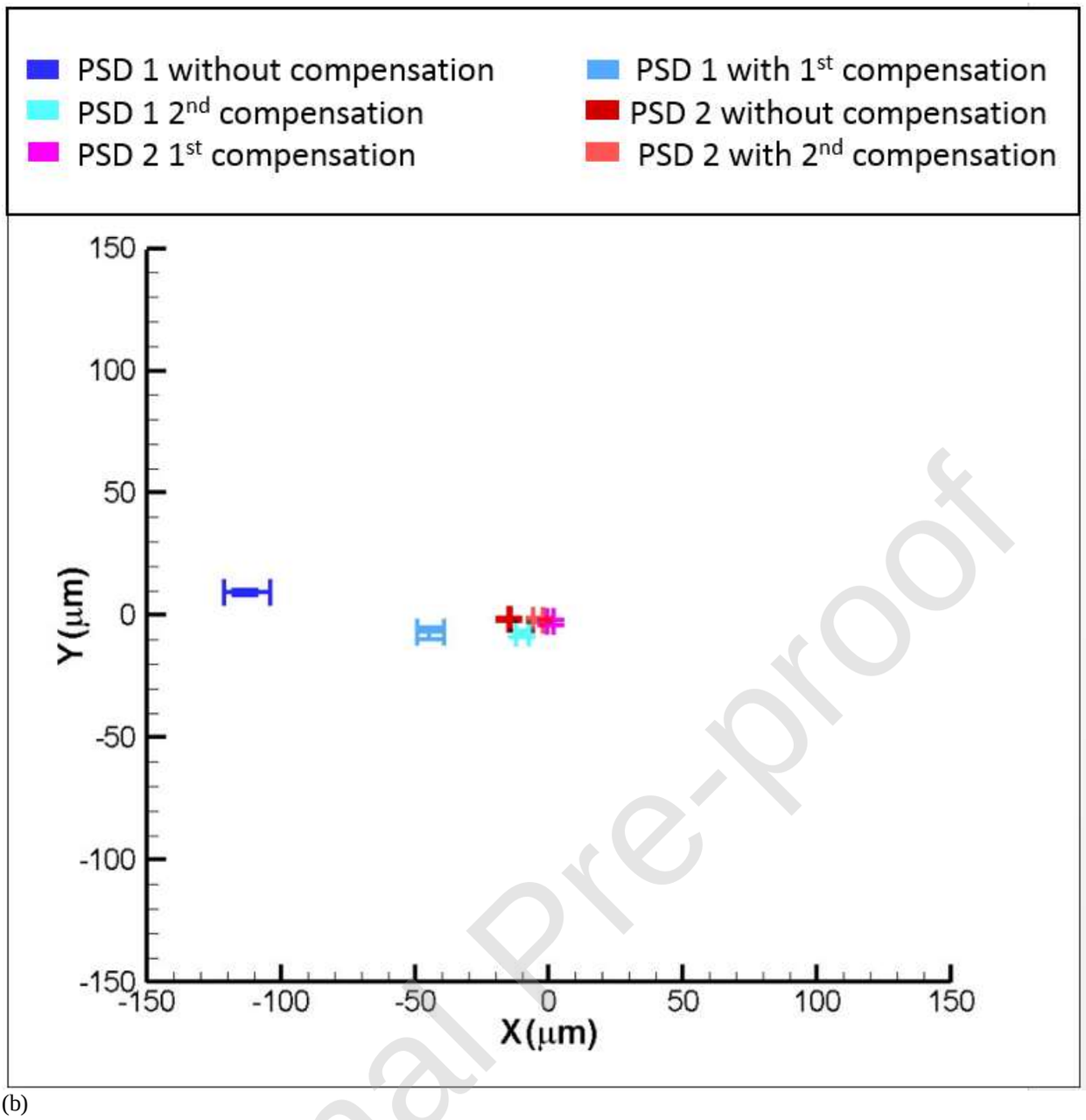


(b)

Figure 18. Experimental results for variation of positions of light spots on PSDs with and without compensation (a) $\theta_y$ = 2.5 mrad and (b) $\theta_y$ = −2.5 mrad, respectively.

## 7. Closed-loop experiment of the proposed 4-DOF FSM

This section will focus on preliminary closed-loop control of the proposed 4-DOF FSM using a PI control method, including the experiments of closed-loop position control and closed-loop frequency response. The prototype used the PSD and laser displacement meter as sensors to detect rotational movement and translational movement during the closed-loop control. Figures 19 and 20 show the experimental results of the closed-loop step response. The rotational and tranlational

Journal Pre-proof

accuracies of the proposed protptye are 0.025 mrad and 0.0012 mm, respectively, which are much better than those of 0.5 mrad and 0.007 mm obtained in the open-loop control, respectively. Figures 21 and 22 show the experimental results of the closed-loop frequency response of prototype. The rotational and translational movements of the prototype have the bandwidths of 10 Hz and 39 Hz, respectively.

The typical commercial FSM (Newport FSM-300-01) that is a 2-axis rotational mechanism used in laser beam stabilization has a travel range of ±26.2 mrad with a bandwidth of 600 Hz. The proposed 4-DOF FSM in this paper has a travel range of ±5 mrad and a bandwidth of 10 Hz for the rotational movement; and has a travel range of ±0.04 mm and a bandwidth of 39 Hz for the translational movement. The frequency response of the proposed 4-DOF FSM is lower than that of the commercial FSM and could not be improved by using the PI control system in the current hardware setup. We infer that it is because the mechanical structure/spring has unexpected deformation during the closed-loop oscillation process. Because we were limited to available materials and fabrication methods, the prototype's mechanical structure is not ideal. The resulting spring plate with a thickness of 0.4 mm is obtained by manually sticking four 0.1 mm plates together. Nevertheless, the performance of the proposed 4-DOF FSM would be improved if we could have a better-fabricated prototype.

Journal Pre-proof

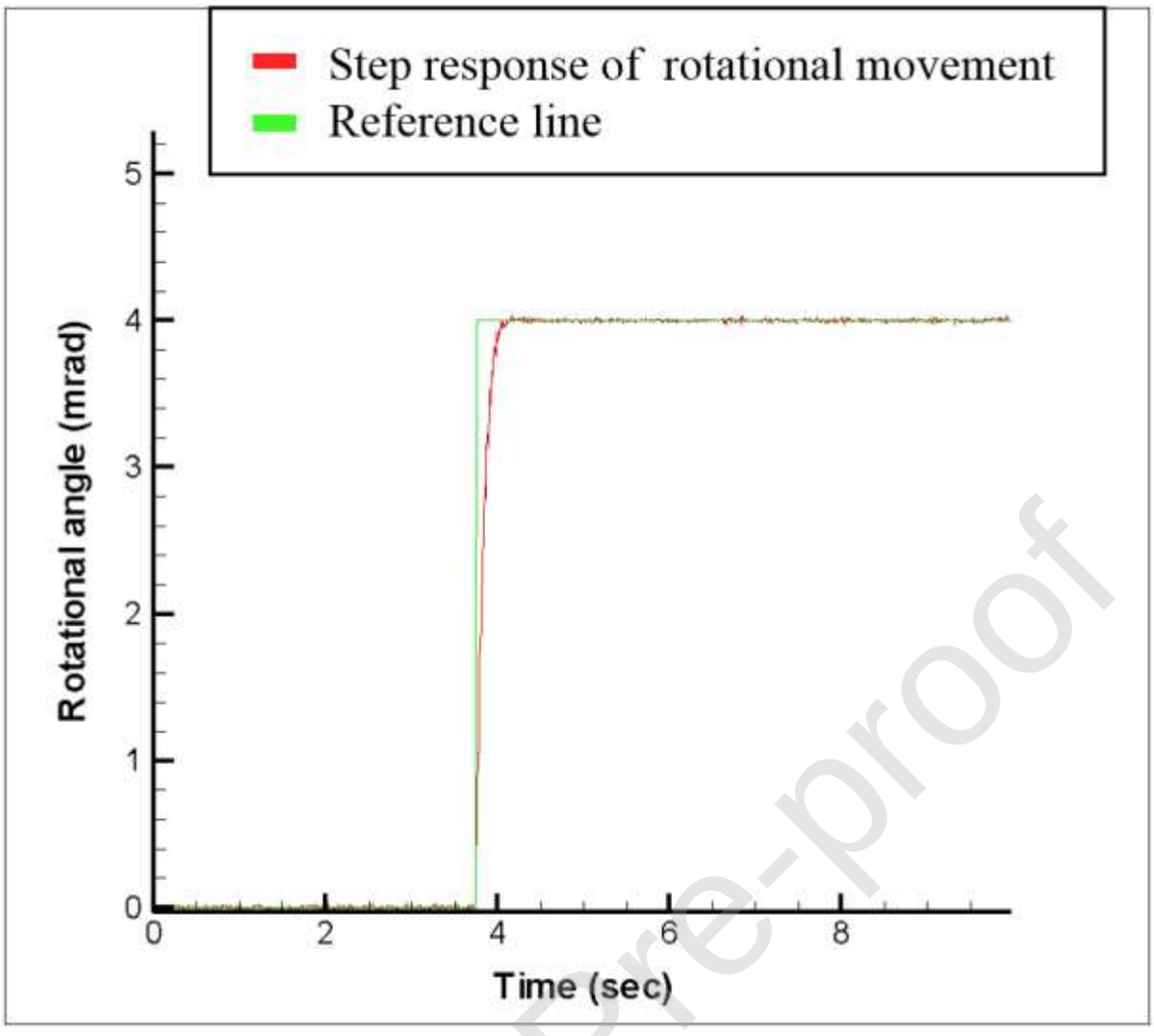


Figure 19. Closed-loop step response of rotational movement.

Journal Pre-proof

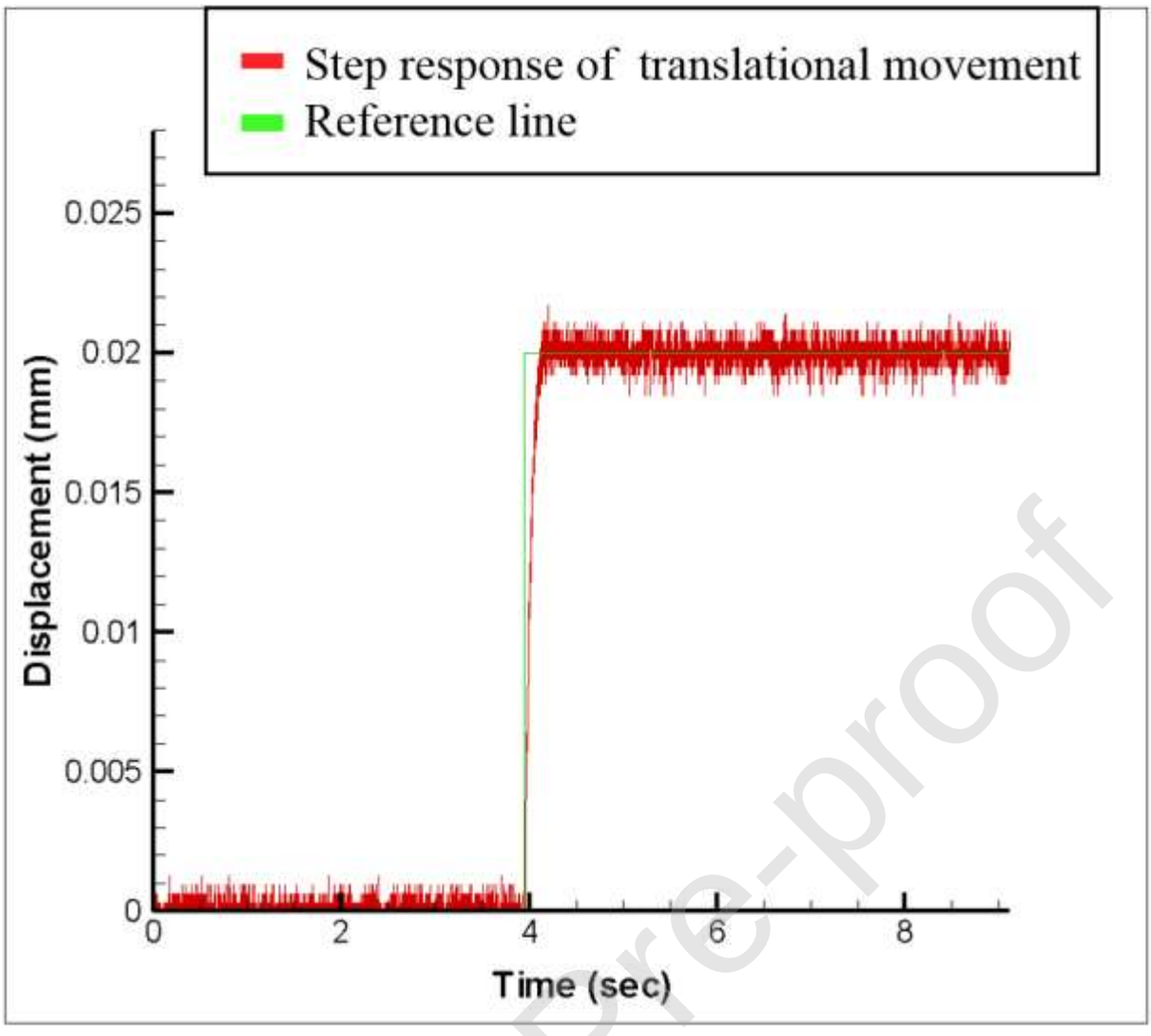


Figure 20. Closed-loop step response of translational movement.

Journal Pre-proof

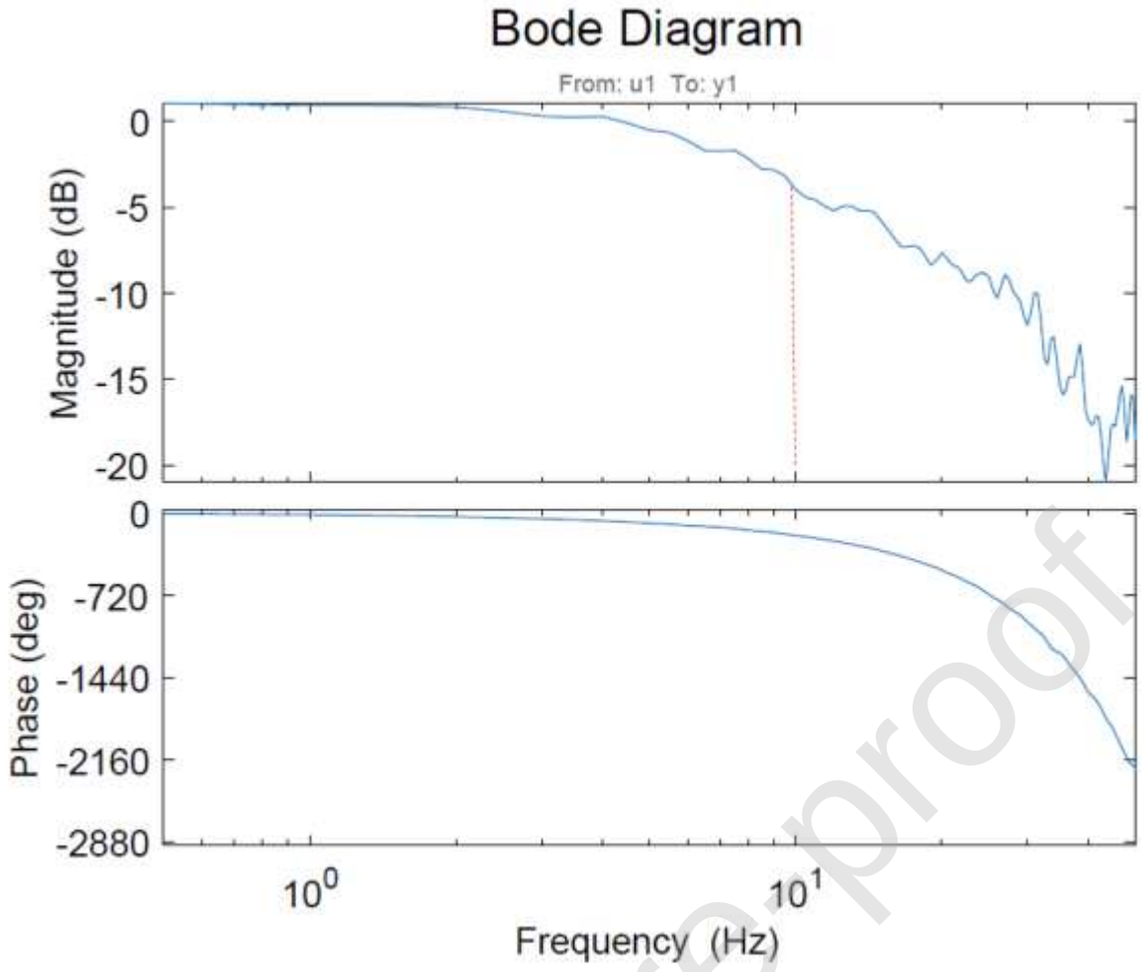


Figure 21. Closed-loop frequency response of rotational movement.

Journal Pre-proof

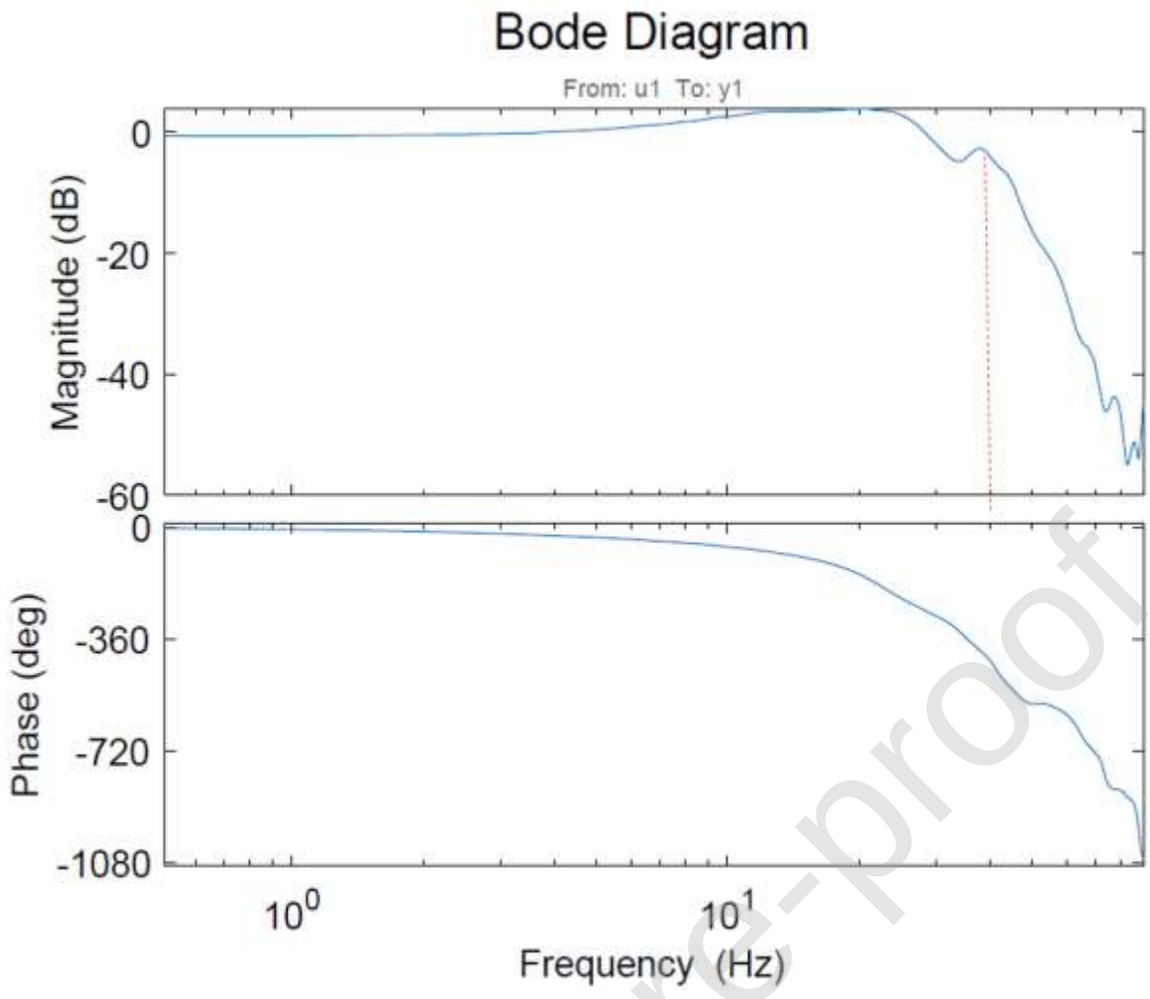


Figure 22. Closed-loop frequency response of translational movement.

## 8. Conclusions

This study has presented a 4-DOF FSM to compensate 4-DOF laser errors. A 4-DOF actuator has been integrated into the proposed 4-DOF FSM. The performance of the proposed 4-DOF FSM has been evaluated by using a laboratory-built prototype. The experiment results show that the proposed 4-DOF FSM has the rotational and translational ranges of ± 5 mrad and ± 0.04 mm along the X and Y axes, respectively, and the bandwidths of 10 Hz and 39 Hz for rotational and translational motions, respectively. The experiment results have demonstrated that the proposed 4-DOF FSM could compensate 4-DOF laser errors with the accuracies of 0.025 mrad and 0.0012 mm for rotational and translational movements, respectively, in the closed-loop control.

Journal Pre-proof

**Author statement**

**Yu-Hao Chang:** Writing- Original draft preparation, Conceptualization, Methodology, Software, Validation. **Guang-bo Hao***:* Conceptualization, Writing- Reviewing and Editing. **Chien-Sheng Liu**: Writing- Reviewing and Editing, Supervision, Project administration.

**Declaration of interests**
The authors declare that they have no known competing financial interests or personal relationships that could have appeared to influence the work reported in this paper.

## Acknowledgements

The authors gratefully acknowledge the financial support provided to this study by the Ministry of Science and Technology of Taiwan under Grant Nos. MOST 105-2221-E-194-013-MY5, 106-2628-E-194-001-MY3, and 108-2218-E-002-071.

## References

[1] R. A. Potyrailo, W. G. Morris, A. M. Leach, T. M. Sivavec, M. B. Wisnudel, and S. Boyette, “Analog signal acquisition from computer optical disk drives for quantitative chemical sensing, ” Anal. Chem. 78, 5893-5899 (2006).

[2] J. Stirnemann, G. Chalouhi, M. Essaoui, N. Bahi-Buisson, P. Sonigo, A-E Millischer, A. Lapillonne, V. Guigue, L. J. Salomon, and Y. Ville, “Fetal brain imaging following laser surgery in twin-to-twin surgery, ” BJOG. 125, 1186-1191 (2018).

[3] D. Kopp, L. Lehmann, and H. Zappe, “Optofluidic laser scanner based on a rotating liquid prism, ” Appl. Opt. 55, 2136-2142 (2016)

[4] K. Tamura , R. Ishigami, and R. Yamagishi, “Laser cutting of thick steel plates and simulated steel components using a 30 kW fiber laser,” J. Nucl. Sci. Technol. 53, 916-920 (2016).

[5] J. Chen, D. N. Wang, A. Ramachandran, S. Chandran, M. Li, and R. Varma, “An open-path dual-beam laser spectrometer for path-integratedurban NO2 sensing,” Sens. Actuator A-Phys. 315, 112208 (2020).

[6] Y. Zhao, Y. L. Zhao, and L. K. Wang,“Application of femtosecond laser micromachining in silicon carbide deep etching for fabricating sensitive diaphragm of high temperature pressure sensor,” Sens. Actuator A-Phys. 309, 112017 (2020).

Journal Pre-proof

[7] H. Klingel, “Laser apparatus with novel beam aligning means and method of laser processing of workpieces using same,” U.S. Patent, 4675501A (1987).

[8] M. N. Sweeney, G. A. Rynkowski, M. Ketabchi, and Robert Crowley, “Design considerations for fast-steering mirrors (FSMs),” in Proc. Int. Symp. Opt. Sci. Technol. Seattle, WA, USA. 63–73(2002).

[9] D. K. Wang, C. Watkins, S. Koppal, and H. K. Xie, “A silicon optical bench with vertically-oriented micromirrors for active beam steering,” Sens. Actuator A-Phys. 298, 111586 (2020).

[10] Y. H. Gong, K. X. Yang, H. L. Yong, J. Y. Guan, G. L. Shentu, C. Liu, F. Z. Li, Y. Cao, J. Yin, S. K. Liao, J. G. Ren, Q. Zhang, C. Z. Peng, and J. W. Pan, “Free-space quantum key distribution in urban daylight with the SPGD algorithm control of a deformable mirror, ” Opt. Express 26, 18897-18905 (2018).

[11] X. Wu, N. Tang, B. Liu, and Z. Long, “A novel high precise laser 3D profile scanning method with flexible calibration,” Opt. Lasers Eng. 132, 105938 (2020).

[12] L. H. Yang, R. Y. Liao, J. R. Lin, B. Sun, Z. Wang, K. Patrick, and J. G. Zhu, “Enhanced 6D measurement by integrating an Inertial Measurement Unit (IMU) with a 6D sensor unit of a laser tracker,” Opt. Lasers Eng. 126, 105902 (2020).

[13] T. Huang, D. Zhao, F. W. Yin, W. J. Tian, and D. G. Chetwynd, “Kinematic calibration of a 6-DOF hybrid robot by considering multicollinearity in the identification Jacobian,” Mech. Mach. Theory 131, 371-384 (2019).

[14] Q. K. Zhou, P. Ben-Tzvi, D. P. Fan, and A. A. Goldenberg, “Design of fast steering mirror systems for precision laser beams steering,” 2008 IEEE Int. Work. Robot. Sensors Environ. 144–149 (2008).

[15] Q. K. Zhou, P. Ben-Tzvi, and D. P. Fan, “Design and analysis of a fast steering mirror for precision laser beams steering,” Sensors & Transducers. 5, Special Issue, 104-118 (2009).

[16] Y. J. Long, J. Q. Mo, X. H. Wei, C. L. Wang, and S. G. Wang, “Design of a moving-magnet electromagnetic actuator for fast steering mirror through finite element simulation method. Journal of Magnetics,” J. Magn. 19, 300-308 (2014).

[17] M. J. Obrien, and W. B Smith, “Fast steer mirror,” U.S. Patent, 8128246B1 (2012).

Journal Pre-proof

[18] M. B. Akbarzadeh, H. Moeenfard, S. Awtarc, "Nonlinear dynamic modeling of a parallelogram flexure," Mech. Mach. Theory 153, 103985 (2020).

[19] T. Liu, S. S. Bi, Y. B. Yao, Z. H. Dong, Q. Z. Yang, and L. Liu, "Research on zero-stiffness flexure hinge (ZSFH) based on spring four-bar linkage (4BSL)," Mech. Mach. Theory 143, 103633 (2020).

[20] K. Wu, and G. B. Hao, "Design and nonlinear modeling of a novel planar compliant parallelogram mechanism with general tensural-compresural beams," Mech. Mach. Theory 152, 103950 (2020).

[21] Y. H. Chang, C. S. Liu, I. W. Chen, M. S. Tsai, and H. C. Tseng, "Open-loop control of voice coil motor with magnetic restoring force using high-low frequency composite signals," IEEE Access, 7, 146258-146263 (2019).

[22] Y. H. Chang, C. J. Lu, C. S. Liu, D. S. Liu , S. H. Chen, T. W. Liao, W. Y. Peng, and C. H. Lin, "Design of miniaturized optical image stabilization and autofocusing camera module for cellphones," Sens. Mater. 29, 989-995 (2017).

[23] C. S. Liu, B. J. Tsai, and Y. H. Chang, "A compact low-cost camera module with modified magnetic restoring force," J. Mech. 33, 475-482 (2017).

[24] R. Lin, Y.Z. Li, Y. G. Zhang, T. W. Wang, Z. Y. Wang, Z. H. Song, Z. P. Dou, and J.Q. Qianac, "Design of a flexure-based mixed-kinematic XY high-precision positioning platform with large range," Mech. Mach. Theory. 142, 103609 (2019).

[25] Y. H. Chang, C. J. Lu, C. S. Liu, D. S. Liu, S. H. Chen, T. W. Liao, W. Y. Peng, and C. H. Lin, "Design of miniaturized optical image stabilization and autofocusing camera module for cellphones," Sens. Mater. 29, 989–995 (2017).

[26] C. L. Hsieh, H. Y. Wang, Y. H. Chang, and C. S. Liu, "Design of VCM actuator with the chamfered edge magnet for cellphone," Microsyst. Technol. 23, 5293-5302 (2017).

[27] C. L. Hsieh, Y. H. Chang, Y. T. Chen, and C. S. Liu, "Design of VCM actuator with L-shape coil for smartphone cameras," Microsyst. Technol. 24, 1033-1040 (2018).

[28] C. L. Hsieh, C. S. Liu, and C. C. Cheng, "Design of a 5 degree of freedom–voice coil motor actuator for smartphone camera modules," Sens. Actuator A-Phys. 309, 112014 (2020).

Journal Pre-proof

[29] Y. H. Chang, C. S. Liu, and C. C. Cheng, "Design and characterisation of a fast steering mirror compensation system based on double porro prisms by a Screw-Ray Tracing method," Sensors 18. 4046. 10.3390/s18114046 (2018).

[30] P.D. Lin, "Advanced Geometrical Optics," Springer: Singapore, 2017.

[31] M. Sugawara, A. Moriya, K. Sato, M. Ariji, and S. Ajiki, "Lens holder driving device including fracture preventing member for suspension wires," U.S. Patent, 20130016428A1 (2013).

**Yu-Hao Chang** received his MS degree from the department of mechanical engineering at National Chung Cheng University, Chiayi, Taiwan, in 2015. He is studying for a doctorate at Department of Mechanical Engineering in the National Chung Cheng University currently, Chiayi, Taiwan. His current research interests include applications of fast steer mirror and voice coil motors.

Dr. **Guangbo Hao** is a Senior Lecturer with University College Cork. He obtained his PhD degree in Mechanical Engineering from Heriot-Watt University in 2011. He is a member of ASME and an elected member of the ASME Mechanisms and Robotics Committee. He is serving as the Editor-in-Chief of the IFToMM affiliated journal: Mechanical Sciences and the Associate Editor of ASME Journal of Mechanisms and Robotics. He has won some accolades including the 2017 and 2018 ASME Compliant Mechanisms Awards in a row. He has published over 130 peer-reviewed publications.

**Chien-Sheng Liu** received his BS and MS degrees from the department of power mechanical engineering at National Tsing Hua University, Hsinchu, Taiwan, in 1996 and 1999, respectively, and his PhD degree from the department of mechanical engineering at National Cheng Kung University, Tainan, Taiwan in 2010. He worked at the Industrial Technology Research Institute (ITRI), Taiwan, as a mechanical design engineer from 2003 to 2011. He was an assistant professor in the department of mechanical engineering at National Central University, Jhongli, Taiwan from 2011 to 2012 and joined the mechanical department at National Chung-Cheng University, Chiayi, Taiwan in 2012. He is currently a professor in the department of mechanical engineering at National Cheng Kung University, Tainan, Taiwan since 2018. His current research interests include applications of force sensors, voice coil motors, spindle motors, fluid dynamic bearing, laser-based auto-focusing module, and opto-electronics sensing.